Chapter 2

OPTICAL KERR EFFECT EXPERIMENTS ON COMPLEX LIQUIDS

A Direct Access to Fast Dynamic Processes

Paolo Bartolini, Andrea Taschin, Roberto Eramo, and Renato Torre

Abstract The time-resolved spectroscopy based on polarization effects represents one of the most sensitive techniques for studying dynamical phenomena in condensed matter. The optical Kerr effect performed with ultra-short laser pulses enables a unique investigation of dynamic processes covering a wide time range, typically from few femtoseconds up to many nanoseconds. This spectroscopic tool is particularly well suited for the measurement of relaxation patterns in complex liquids where several dynamic phenomena, taking place on different time scales, are present. In this chapter we introduce the optical Kerr effect principles, the experimental procedure, and some results from measurements in a number of different complex liquids.

2.1 Introduction

Since 1875, thanks to Kerr's discovery [1], it is known that a static electric field can induce a modification of the optical properties of a liquid. Many years later researchers found out that also an optical electromagnetic field was capable of producing a measurable modification of the dielectric properties, inducing a birefringence effect: the first experimental observation of the optical Kerr effect (OKE) was reported in 1963 [2]. After few years, with the introduction of the first pulsed lasers, spectroscopists discovered the chance to induce in a material a transient birefringence and to measure its relaxation toward the equilibrium [3]. They also realized that this could be a relevant new spectroscopic tool able to collect new information on the dynamical processes present in the material. The spectroscopic research, worked out in the following years, confirmed this forecast beyond the expectations. Two important experimental improvements of this spectroscopic technique have been made. On one hand, the pulsed laser sources have become able to produce very short pulses of high

energy in a very reliable way, on the other hand the introduction of the optical heterodyne detection has improved substantially the quality of the OKE data in terms of signal/noise ratio [4] and control of spurious birefringence effects in the signal [5]. During the 80s the first OKE experiments utilizing subpicosecond laser pulses with heterodyne detection were presented [6, 7]. These pioneering works defined the real possibility of the optical Heterodyne Detected Optical Kerr Effect (HD-OKE) in investigating the fast dynamics of simple molecular liquids, and it opened the way to a series of new experimental HD-OKE studies [8–21].

Recently, the OKE technique has been utilized to investigate the dynamics of more complex liquids, like molecular liquids approaching a phase transition [22], liquid crystals [23] and glass-formers [24]. To perform a correct and complete spectroscopic study of these complex systems, the OKE needs to be performed with heterodyne detection [25, 26] over a very large time window; these requirements forced researchers to develop new experimental procedures [26–30]. From these studies clearly arises the need for a more detailed understanding of the general problem of the interaction of the laser pulses with the molecular liquids and the following induced effects, often common to other time-resolved techniques [31–35], see also Chap. 3. All these time-resolved spectroscopic investigations made clear that the study of relaxation phenomena in the time domain gives valuable information, which is complementary to the frequency domain measurements. This is particularly valuable when complex decay patterns and a variety of relaxation channels are present. In some respects, the development of new time-resolved spectroscopies gives also a renew relevance to the HD-OKE experiments that are still able to produce very interesting results on well-studied molecular liquids [36, 37]. In the first Section, we introduce the basic principle of OKE experiments defining the measured signal. In Sect. 2.3, we analyze the OKE response function and its connection with some theoretical models of liquid dynamics. In Sect. 2.4, we present the experimental procedure and set-up implemented by the authors. In the last Section, we summarize some experimental results on simple and complex liquids.

2.2 Time-Resolved OKE Experiments

When a laser pulse passes through a material it produces a local non equilibrium state that induces a modification of the optical properties. This is a transient effect that relaxes back to the equilibrium state through a variety of processes. In a typical pump-probe experiment, a second laser pulse is sent on the material probing the optical modifications induced by the pump pulse. Since the second laser pulse arrives with a controlled delay, it monitors and measures the transient optical excitation and hence the relaxation of the nonequilibrium state. In the time-resolved OKE both the pulses, pump and probe, are linearly

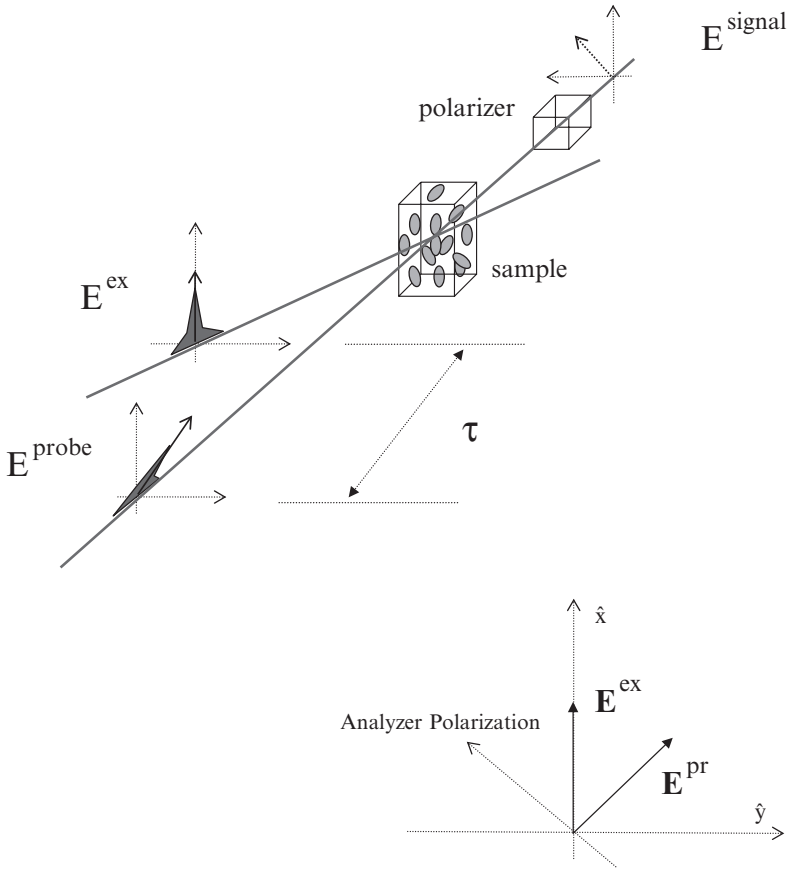

Fig. 2.1 The laser pulse and sample configuration used in a typical OKE experiment

polarized and nonresonant with any electronic state. The pump pulse induces in an isotropic medium (e.g. a liquid or glass) a transient optical anisotropy, as it modifies the index of refraction along the spatial axis parallel to the pump polarization direction, see Fig. 2.1. When no absorption of the laser field is present, just the real part of the refractive index is modified and this effect is called induced birefringence. On the other hand, if a laser absorption is present, also the imaginary part of the refractive index is modified and the effect is called induced dichroism [5]. In this chapter, we will focus only on transparent complex liquids, i.e. electronically nonresonant liquids. Indeed, for completeness, we must note that recently the presence of a very weak dichroic contribution in the HD-OKE signal has been reported also in a medium without any electronic resonance [38] and, moreover, it has been reported that also other type of resonances, as overtones and/or combinations of vibrational bands, could induce a

birefringence in the sample [31]. Nevertheless, we will assume in the following that these contributions are negligible in a properly optimized OKE experiment.

2.2.1 A Simple Model

The physical processes describing the field–matter interaction in an OKE experiment are quite complicated and they are defined properly by the nonlinear optics equations [39–41]. In the next chapter, we will outline the rigorous description of the experiment based on the four-wave mixing phenomena equations. Here we introduce a relatively simple model of the OKE experiment, either continuous or time-resolved, that retains all the principal features. This model is based on few intuitive starting approximations that will be proved later. The first basic approximation is the separation between excitation and the probing processes.

2.2.1.1 The Excitation Process

The first laser pulse is linearly polarized in the $\hat{x}$ direction, see Fig. 2.1, and it can be described during its propagation in the sample, according to the following equation, see also the appendix:

$$\mathbf{E}^{\mathrm{ex}}(z,t) = \hat{\mathrm{e}}_x \mathcal{E}^{\mathrm{ex}}(z,t)\, \mathrm{e}^{\mathrm{i}\omega(\frac{\eta_0}{c}z - t)}, \tag{2.1}$$

where η_0 is the equilibrium isotropic index of refraction of the sample. This pulse propagates in the material producing a transient linear birefringence. The laser pulse modifies the real part of the index of refraction, introducing a small anisotropic variation. As a first approximation, we can write the new excited-state refractive index as follows:

$$\eta_{ij}(\tau) = \eta_0 + \Delta\eta_{ij}(\tau), \tag{2.2}$$

$$\Delta\eta_{ij}(\tau) = \begin{pmatrix} \Delta\eta_{xx}(\tau) & 0 \\ 0 & \Delta\eta_{yy}(\tau) \end{pmatrix}, \tag{2.3}$$

where $\Delta\eta_{ij}$ is the transient birefringence induced by the laser excitation pulse and the i and j indicate the direction of polarization and τ is the delay time between the excitation and probing times. We suppose here non overlapping pulses (i.e. $\tau > 0$) and a medium response time longer than the pulse duration. In the present experimental configuration, because of the initial isotropy of the medium, only the xx (parallel to the excitation) and the yy (perpendicular to the excitation) matrix elements are modified by the excitation beam. The induced anisotropy is defined by the interaction between the excitation pulse and the material; if this is nonresonant the following equation holds:

$$\Delta\eta_{ij}(\tau) \propto \int \mathrm{d}t' \mathcal{R}_{ijxx}(\tau - t') I_{\mathrm{ex}}(t'), \tag{2.4}$$

where $I_{\mathrm{ex}} \propto |\mathcal{E}_x^{\mathrm{ex}}(z,t)|^2$ is the intensity of the laser pulse and $\mathcal{R}_{ijxx}(t)$ is the material response function that defines how the optical properties of the material

are modified by the excitation laser pulse (that in the present case has the $\hat{\mathrm{e}}_x$ linear polarization, see (2.1)). Furthermore, the response function defines which modes are excited in the material, by the field–matter interaction, and how these modes evolve in time according to the material dynamics. This function is indeed the more relevant observable to be measured in a time-resolved spectroscopic experiment. In the following chapters, we will analyze the response function in detail as well how this is connected with molecular dynamics present in the materials.

2.2.1.2 The Probing Process

After the sample has been excited, the probe beam propagates in the sample probing the modified index of refraction. We assume the probe beam linearly polarized at 45° with respect to the excitation beam in the $\hat{xy}$ plane. The expression of the laser beam before the sample has been reported in the appendix. After the beam has propagated through the sample, the anisotropic index of refraction produces a modification of phase, which is different for the probe components along $\hat{x}$ and $\hat{y}$. Neglecting the effect of the induced birefringence (see appendix) on the probe envelope functions, $\mathcal{E}$, the expression for the probe electric field after the sample is

$$\begin{aligned}
\mathbf{E}^{\mathrm{pr}}(z,t) &= \hat{\mathrm{e}}_x E_x^{\mathrm{pr}}(z,t) + \hat{\mathrm{e}}_y E_y^{\mathrm{pr}}(z,t),\\
E_x^{\mathrm{pr}}(z,t) &= \mathcal{E}^{\mathrm{pr}}(z,t)\, \mathrm{e}^{\mathrm{i}\phi_{xx}(\tau)}\, \mathrm{e}^{\mathrm{i}\omega(\frac{z}{c}-t)},\\
E_y^{\mathrm{pr}}(z,t) &= \mathcal{E}^{\mathrm{pr}}(z,t)\, \mathrm{e}^{\mathrm{i}\phi_{yy}(\tau)}\, \mathrm{e}^{\mathrm{i}\omega(\frac{z}{c}-t)},
\end{aligned} \tag{2.5}$$

where the phase modification produced by the sample, $\phi(\tau)$, according to Eq. (2.3), can be written as:

$$\begin{aligned}
\phi_{xx}(\tau) &= \frac{\omega l}{c}\eta_{xx}(\tau) = \frac{\omega l}{c}(\Delta\eta_{xx}(\tau) + \eta_0),\\
\phi_{yy}(\tau) &= \frac{\omega l}{c}\eta_{yy}(\tau) = \frac{\omega l}{c}(\Delta\eta_{yy}(\tau) + \eta_0),
\end{aligned} \tag{2.6}$$

where l is the sample length in the $\hat{z}$ direction. The previous equations, (2.5) and (2.6), describe the beam after the propagation through the excited sample. Successively, the probe beam is analyzed by a polarizer crossed with the input probe beam polarization, i.e. -45° with respect to the excitation beam. The beam exciting the crossed polarizer represents the signal field measured in an OKE experiment, $\mathbf{E}^{\mathrm{sg}}(z,t)$. The effect of the analysis polarizer is to project the

components of the probe beam according to the following expression [1]:

$$\begin{aligned}\mathbf{E}^{\mathrm{sg}}(z,t) &= (\hat{\mathrm{e}}_x - \hat{\mathrm{e}}_y)[E_x^{\mathrm{pr}}(z,t) - E_y^{\mathrm{pr}}(z,t)] \\ &= (\hat{\mathrm{e}}_x - \hat{\mathrm{e}}_y)[\mathrm{e}^{\mathrm{i}\phi_{xx}(\tau)} - \mathrm{e}^{\mathrm{i}\phi_{yy}(\tau)}]\mathcal{E}^{\mathrm{pr}}(z,t)\ \mathrm{e}^{\mathrm{i}\omega(\frac{z}{c}-t)} \\ &= (\hat{\mathrm{e}}_x - \hat{\mathrm{e}}_y)\ \mathrm{e}^{\mathrm{i}\frac{\omega l}{c}\eta_0}[\mathrm{e}^{\mathrm{i}\frac{\omega l}{c}\Delta\eta_{xx}(\tau)} - \mathrm{e}^{\mathrm{i}\frac{\omega l}{c}\Delta\eta_{yy}(\tau)}]\mathcal{E}^{\mathrm{pr}}(z,t)\ \mathrm{e}^{\mathrm{i}\omega(\frac{z}{c}-t)},\end{aligned} \tag{2.7}$$

where we used (2.6). Considering that the induced variation $\Delta\eta(t)$ is a small effect and showing explicitly only the time-dependent parameters, we can approximate the previous equation as follows:

$$\begin{aligned}E^{\mathrm{sg}}(z,t) &\propto \mathrm{i}\ [\Delta\eta_{xx}(\tau) - \Delta\eta_{yy}(t)]\ \mathcal{E}^{\mathrm{pr}}(z,t)\ \mathrm{e}^{\mathrm{i}\omega(\frac{z}{c}-t)} \\ &\propto \mathrm{i}\ [\int \mathrm{d}t'\ \mathcal{R}_{\mathrm{oke}}(\tau - t')\mathcal{I}(t')]\ \mathcal{E}^{\mathrm{pr}}(z,t)\ \mathrm{e}^{\mathrm{i}\omega(\frac{z}{c}-t)},\end{aligned} \tag{2.8}$$

where $\mathcal{R}_{\mathrm{oke}} = \mathcal{R}_{xxxx} - \mathcal{R}_{yyxx}$ and $\mathcal{I}(t) \propto [\mathcal{E}(t)]^2$, begin $\mathcal{E}(t)$ the envelope describing the main laser pulse, see appendix. Equation (2.8) defines the signal beam measured in an OKE experiment and it shows that the dynamical information of the material are obtained through the measured response function. In the present derivation we supposed well separated pulses, neglecting the instantaneous electronic contribute. This can be taken into account for a sufficiently thin medium in order to neglect pulse spreading and slipping effects: the final result is that, in Eq. 2.8, $\mathcal{R}_{\mathrm{oke}}(\tau - t')$ should be replaced by $\mathcal{R}_{\mathrm{oke}}(t - t')$.

The signal electromagnetic wave can be detected using two different experimental schemes: the homodyne or the heterodyne detection. In the first detection scheme, the signal beam is sent to a square law detector, typically a photomultiplier or a photodiode followed by a current integrator. In this case, the measured signal can be written according to the following expression:

$$S_{\mathrm{homo}}(\tau) \propto \int |E^{\mathrm{sg}}(t)|^2\ \mathrm{d}t \propto \int \mathrm{d}t\mathcal{I}(t-\tau)[\int \mathrm{d}t'\mathcal{R}_{\mathrm{oke}}(t-t')\mathcal{I}(t')]^2, \tag{2.9}$$

In the heterodyne detection scheme, that will be described in detail in Sect. 2.4.1, the signal field is superimposed with a local field so that the measured signal is linearly connected with the material response. In this case, see also (2.62), the signal can be written as

$$S_{\mathrm{hete}}(\tau) \propto \int \mathrm{d}t\mathcal{I}(t-\tau) \int \mathrm{d}t'\mathcal{R}_{\mathrm{oke}}(t-t')\mathcal{I}(t'). \tag{2.10}$$

If the pulse durations are short compared to the timescales of material dynamics, the intensity can be approximated as $\mathcal{I}(t) \simeq \mathbb{I}\delta(t)$ and so the OKE experiments measure directly in the time domain the response function:

$$S_{\mathrm{homo}}(\tau) \propto [\mathcal{R}_{\mathrm{oke}}(\tau)]^2\mathbb{I}_{\mathrm{pr}}\mathbb{I}_{\mathrm{ex}}^2, \tag{2.11}$$

$$S_{\mathrm{hete}}(\tau) \propto \mathcal{R}_{\mathrm{oke}}(\tau)\mathbb{I}_{\mathrm{pr}}\mathbb{I}_{\mathrm{ex}}. \tag{2.12}$$

We would like to stress how the time resolution in this OKE experiment is determined by the laser pulse duration. Indeed, other experimental parameters are important, as we will see in Sect. 2.4, e.g. the optical delay line that defines the delay τ. So if short laser pulses are available, fast dynamic phenomena can be directly revealed and measured in the time domain.

2.2.2 The Nonlinear Optics Framework

The basic equations describing the OKE can be introduced within the framework of nonlinear optics and spectroscopy [39–41].

In this approach, the interaction of an electromagnetic field, E, with the matter is described on the basis of a series expansion of field power. So basically the polarization induced in a medium is the sum of separated effects that are linear, quadratic, cubic, and so on, in E. Each of these effects shows a variety of phenomena that can be isolated and described by the nonlinear optics framework. The optical Kerr effect is a third-order nonlinear process (i.e. it is produced by the cubic term in the polarization expansion); more specifically it is a four-wave mixing process. Two waves are associated with the excitation laser, thus acting twice in the field expansion, and a third wave with the probe beam. These three electromagnetic waves interact in the material producing a third-order polarization, via the third-order susceptibility. The nonlinear polarization is source of a new electromagnetic field that represents the fourth wave and the signal from the spectroscopic point of view, differing by the probe beam only for the polarization state.

The third-order polarization can be written as [40]

$$P_i^{(3)}(t) = \sum_{jkl} \int \mathrm{d}t_1 \int \mathrm{d}t_2 \int \mathrm{d}t_3 \; \mathcal{R}_{ijkl}^{(3)}(t-t_1, t-t_2, t-t_3) E_j(t_1) E_k(t_2) E_l(t_3), \quad (2.13)$$

where $P_i^{(3)}$ is the ith component of the third-order polarization, $\mathcal{R}^{(3)}$ is the general third-order response tensor of the material. In (2.13) we assumed that the macroscopic nonlinear polarization density, $P^{(3)}(\mathbf{r}, t)$, depends locally only on the field, $E(\mathbf{r}, t)$, at its own position $\mathbf{r}$. With this assumption we have omitted the reference to $\mathbf{r}$ in the response tensor $\mathcal{R}^{(3)}$ [41].

The $\mathcal{R}^{(3)}$ tensor is a very complex function that defines the coupling of the optical electromagnetic fields with the material and how these are modified by the structural and dynamical properties of the medium. In the general definition of such tensor many nonlinear optical phenomena are included. A full description of this physical property is a tremendous task even at the simpler level. Nevertheless, a few general properties and some approximations help in partially reducing the $\mathcal{R}^{(3)}$ complexity.

As previously introduced, we are focusing on the nonresonant OKE where all the laser pulses, excitation, and probe are characterized by the same frequency not resonant with any material electronic state. In this case the Born-Oppenheimer (B-O) approximation is valid and a simplified expression for the third-order response can be introduced [41]:

$$\mathcal{R}^{(3)}_{ijkl}(t-t_1,t-t_2,t-t_3) = \gamma^{(e)}_{ijkl}\delta(t-t_1)\delta(t-t_2)\delta(t-t_3) + \mathcal{R}^{(\mathrm{nucl})}_{ijkl}(t-t_2)\delta(t-t_1)\delta(t_2-t_3). \quad (2.14)$$

The third-order response can be divided in an instantaneous response due to the electronic hyperpolarizability plus a second noninstantaneous response defined by the nuclear dynamics and hence by the molecular dynamics. This second part includes all the relevant dynamic information in a complex liquid. The proper definition of the nuclear response function will be introduced later, here we recall only the symmetry rules that must be verified by it. In an isotropic medium, as a liquid or a glass, $\mathcal{R}^{(\mathrm{nucl})}$ is subject to several symmetry rules [41]. According to our experimental geometry, there are 8 nonvanishing tensor elements, but only 2 independent components:

$$\begin{aligned} &\mathcal{R}^{(\mathrm{nucl})}_{xxxx} = \mathcal{R}^{(\mathrm{nucl})}_{yyyy}\ ,\ \mathcal{R}^{(\mathrm{nucl})}_{xxyy} = \mathcal{R}^{(\mathrm{nucl})}_{yyxx} \\ &\mathcal{R}^{(\mathrm{nucl})}_{xyxy} = \mathcal{R}^{(\mathrm{nucl})}_{yxyx} = \mathcal{R}^{(\mathrm{nucl})}_{yxxy} = \mathcal{R}^{(\mathrm{nucl})}_{xyyx} = \frac{1}{2}(\mathcal{R}^{(\mathrm{nucl})}_{xxxx} - \mathcal{R}^{(\mathrm{nucl})}_{yyxx}). \end{aligned} \quad (2.15)$$

The general definition of third-order polarization (2.13) is simplified by the B-O approximation, hence using the response definition reported in (2.14) we get [41]

$$\begin{aligned} P^{(3)}_i(t) &= \gamma^{(e)}_{ijkl}E_j(t)E_k(t)E_l(t) \\ &\quad + E_j(t)\int \mathrm{d}t'\mathcal{R}^{(\mathrm{nucl})}_{ijkl}(t-t')E_k(t')E_l(t'). \end{aligned} \quad (2.16)$$

This expression is still quite a general definition that can be further simplified in order to describe the OKE experiments.

In the present OKE experiment, the electromagnetic fields are characterized by the same frequency and wave-vector with different polarization states. Furthermore, we can assume the B-O separation as reported in (2.16). So, neglecting the instantaneous electronic response, considering the time separation between excitation and probe pulses, and verifying the phase matching conditions and the energy conservation, the induced polarization becomes [40]

$$\begin{aligned} P^{(3)}_i(t) &= E^{\mathrm{pr}}_j(t)\Delta\chi_{ij}(t), \\ \Delta\chi_{ij}(t) &= \int \mathrm{d}t'\mathcal{R}^{(\mathrm{nucl})}_{ijxx}(t-t')E^{\mathrm{ex}}_x(t')[E^{\mathrm{ex}}_x(t')]^*, \end{aligned} \quad (2.17)$$

where we assume a sum over repeated indexes. This equation proves that a separation between the excitation process and the probing process, see Sect. 2.2.1, is correct. Furthermore, the second equation is equivalent to (2.4) reported in the previous section.[2] In a general case, when resonant and nonresonant laser interactions are present, $P^{(3)}(t)$ has a different phase from the probe beam. The part of $P^{(3)}(t)$ that is in-phase defines the birefringence, whereas the part that is $\pi/2$ out-of-phase describes the dichroic effect. This separation of the two polarization contributions together with heterodyne detection (see Sect. 2.4.1) allows disentanglement of the birefringence from the dichroic signal: when the local oscillator is $\pi/2$ out-of-phase with the probe, only the birefringence signal is detected; if the local oscillator is in phase only the dichroic signal is measured [7].

Introducing now the probe and excitation field polarizations, according to the experimental configuration shown in Fig. 2.1, and the symmetry rules on the nonlinear response valid for an isotropic medium, see Eq. (2.15), the induced polarization components are

$$\begin{aligned}
\mathbf{P}^{(3)}(t) &= \hat{\mathrm{e}}_x P_x^{(3)}(t) + \hat{\mathrm{e}}_y P_y^{(3)}(t), \\
P_x^{(3)}(t) &= E_x^{\mathrm{pr}}(t') \int \mathrm{d}t' \mathcal{R}_{xxxx}(t-t') |E_x^{\mathrm{ex}}(t')|^2, \\
P_y^{(3)}(t) &= E_y^{\mathrm{pr}}(t') \int \mathrm{d}t' \mathcal{R}_{yyxx}(t-t') |E_x^{\mathrm{ex}}(t')|^2,
\end{aligned} \tag{2.18}$$

where we have omitted the (nucl) superscript in order to simplify the notation.

As already mentioned, the third-order polarization induced in the material produces the fourth field: $\mathbf{E}^{4\mathrm{th}}$. This field is defined by the differential equation that defines the wave propagation in the medium, where $P^{(3)}$ is the source term [40]. According to an approximated solution of this equation we found that $\mathbf{E}^{4\mathrm{th}} \propto i\mathbf{P}^{(3)}$. In other words, the 4^{th} electromagnetic field is the probe beam modified by the excited material and it corresponds to (2.5) previously derived. Following the present experimental configuration, the polarization state of this field is analyzed by a crossed polarizer, see Fig. 2.1. The output field is the measured signal field, $\mathbf{E}^{\mathrm{sg}}$. This optical device produces a projection of the $\mathbf{E}^{4\mathrm{th}}$ polarization components, so that the following signal field results:

$$\mathbf{E}^{\mathrm{sg}}(t) \propto \mathrm{i}(\hat{\mathrm{e}}_x - \hat{\mathrm{e}}_y) E^{\mathrm{pr}}(t) \int \mathrm{d}t' [\mathcal{R}_{xxxx}(t-t') - \mathcal{R}_{yyxx}(t-t')] |E_x^{\mathrm{ex}}(t')|^2, \tag{2.19}$$

where the E^{pr} is the original probe beam (i.e., before it passes through the material). Hence, considering the following definition, derived from the symmetry rules

$$\mathcal{R}_{\mathrm{oke}}(t) \propto \mathcal{R}_{xyxy}(t) = \frac{1}{2}[\mathcal{R}_{xxxx}(t) - \mathcal{R}_{yyxx}(t)], \tag{2.20}$$

and the probe and excitation laser pulses expressions, see (2.A.4) in the appendix, the previous equation can be further simplified to

$$\mathbf{E}^{\mathrm{sg}}(t) \propto \mathrm{i}\,(\hat{\mathrm{e}}_x - \hat{\mathrm{e}}_y)\,\mathcal{E}^{\mathrm{pr}}(t)\,\mathrm{e}^{i\omega(\frac{z}{c}-t)} \int \mathrm{d}t'\,\mathcal{R}_{\mathrm{oke}}(t-t')[\mathcal{E}_x^{\mathrm{ex}}(t')]^2. \quad (2.21)$$

This equation shows how the signal field, according to the introduced approximations, is a plane wave with a slowly varying envelope, see appendix, and it is equivalent to (2.8).

So we found that the nonlinear optics model provides a rigorous description of OKE experiment, where all the relevant approximations are physically defined. We would like to stress again, that the B-O approximation is indeed fundamental. We also showed that this nonlinear optics model explains the basic hypothesis introduced in the simple model, previously described.

2.3 The Response Function

All the material information measurable in a OKE experiment are contained in the third-order response, $\mathcal{R}^{(3)}$, introduced in the previous Sect. 2.2.2. When a nonresonant experiment is performed the Born-Oppenheimer approximation applies and the relevant function becomes the material response, $\mathcal{R}_{ijkl}$, see (2.14) and (2.17). In the B-O model, the response function can always be directly connected with the time-dependent correlation function of the quantum linear susceptibility, χ_{ij}, [41]:

$$\mathcal{R}_{ijkl}(q,t) \propto \frac{\mathrm{i}}{\hbar}\,\theta(t)\,\langle[\chi_{ij}(q,t)\;,\;\chi_{kl}(-q,0)]\rangle\,, \quad (2.22)$$

where $[\cdot]$ is the commutator, the $\langle\cdot\rangle$ is the ensemble average, and $\theta(t)$ the Heaviside step function. This expression in the classical limit becomes

$$\mathcal{R}_{ijkl}(q,t) \propto -\frac{\theta(t)}{k_{\mathrm{B}}T}\frac{\partial}{\partial t}\,\langle\chi_{ij}(q,t)\;\chi_{kl}(-q,0)\rangle\,, \quad (2.23)$$

where k_{B} is the Boltzmann constant and T is the temperature, and we replaced the quantum linear susceptibility with the classical susceptibility tensor. For the sake of simplicity, we wrote the full susceptibility functions in the previous expressions, but we should recall that only the time dependent or fluctuating part, $\delta\chi_{ij}$, is relevant for the response functions. Often in the literature the susceptibility is replaced by the full dielectric tensor since their fluctuating part coincide: $\delta\varepsilon_{ij} = 4\pi\delta\chi_{ij}$, in the CGS units.

Indeed the B-O approximation produces a relevant simplification of the $\mathcal{R}^{(3)}$ tensor. It allows a separation of the electronic and nuclear responses (see (2.14)) and to express the latter in a useful way (2.23). Nevertheless, the $\chi_{ij}(q,t)$ tensor remains a very complex physical variable that can be detailed only using severe approximations, as we will see later.

In the previous equations, we reported the general response function depending also on the wave-vector q; this dependence was neglected in all the previous expressions since this aspect is not relevant in the OKE experiments. In fact in any scattering experiment, linear or nonlinear, the measured signal is defined through the space integration over the sample volume. This integration turns out to be a Fourier-transformation of the response function from the real space, r coordinates, to the reciprocal space, q wave-vectors. So $\mathcal{R}^{(3)}_{ijkl}$ is a time-q dependent function, where the q value is defined by the experimental configuration. As will be detailed in the next chapter, the phase matching condition defines the relation between the angles of the interacting electromagnetic fields, in particular the angle between the two excitation fields, defining the q vector value. In the OKE technique, they are indeed the same field acting twice, so this angle is zero and consequently the wave-vector is zero. So only the response function characterized by $q{\sim}0$ is active in the OKE experiments. This is the reason why we do not report the q-dependence in the equations introduced in the previous paragraphs. A different situation is present in the light scattering (LS) experiments, see [42], or in the transient grating experiment, see Chap. 3. In the former, q is defined by the scattering angle. In the latter it is defined, as in the OKE, by the angle formed by the two excitation fields. In a transient grating, these have different directions of propagation, so the response function is characterized by a nonzero wave-vector.

Expression (2.23) of the response function shows that this experiment verifies the linear response theorem [43]. In fact, when the excitation fields are not resonant and relatively weak, the response is defined by the equilibrium fluctuations, hence the response features are not dependent on the excitation fields' intensities. The validity of this linear approximation can be directly checked in the experiments by measuring the response pattern at different excitation intensities and verifying that it does not change.

As we showed, cf. (2.23) and (2.20), the dynamic observable in an OKE experiment, and also in the forward depolarized light scattering (see also Sect. 2.4.2) is the correlation of the susceptibility or dielectric fluctuations:

$$\Phi^{\mathrm{oke}}_{\chi\chi}(t) = \langle \chi_{xy}(t)\, \chi_{xy}(0) \rangle \,. \tag{2.24}$$

The optically accessible dynamical information on the material is contained in the susceptibility tensor, $\chi_{ij}(q,t)$, and the correlation of its fluctuation. This tensor is a very complex material property. We have to deal with two problems. The first one concerns the proper definition of the tensor on the basis of the fundamental physical parameters of the material. The second challenge is the construction of a theoretical model able to describe the dynamics of such physical parameters. Both are typical many-body problems that can be undertaken only using strong approximations. Here we just want to introduce some

basic models, useful to describe the susceptibility tensor dynamics in complex liquids [42, 44, 45].

2.3.1 The Linear Susceptibility Tensor and Its Correlation

The basic physical models of the susceptibility tensor,[3] which are indispensable to connect the response function with the dynamics of simple and complex liquids, will be described here.

The susceptibility tensor can be separated into two main contributions [42,44]:

$$\chi_{ij}(q,t) = \chi_{ij}^{\mathrm{IM}}(q,t) + \chi_{ij}^{\mathrm{II}}(q,t), \tag{2.25}$$

χ^{IM} describes the Isolated-Molecule term, the χ_{ij}^{II} represents the Interaction-Induced. The first term is defined on the basis of the polarizability of the individual molecule,[4] the second term describes the modification of the χ tensor generated by the intermolecular effects. This interaction can be described at the simplest approximation by the dipole-induced-dipole phenomena. The contributions to the tensor of the II effects, and hence to the measured signals, are typically weak in the liquids formed by molecules with anisotropic polarizability, even if their effects can not be neglected a priori [42, 44]. Indeed, the II is a complex phenomena and in the molecular liquids it can be calculated only numerically by computer simulation [46, 47]. To introduce a simple view we will not explicitly consider the II in this chapter. So in the following we will approximate

$$\chi_{ij}(q,t) \simeq \chi_{ij}^{\mathrm{IM}}(q,t). \tag{2.26}$$

The χ^{IM} tensor can be described on the basis of different theoretical approaches. Here we introduce the two more relevant ones with the aim of describing the response function in complex liquids. One model uses a microscopic approach and it starts from the molecular parameters. The other applies a coarse-graining procedure introducing a few mesoscopic or hydrodynamic variables.

2.3.1.1 The Microscopic Variables

The susceptibility tensor, according to the IM approximation, can be directly connected with the molecular parameters in the reciprocal space [42, 44]:

$$\chi_{ij}(q,t) \simeq \sum_n \alpha_{ij}^n(t)\, \mathrm{e}^{\mathrm{i}q\cdot r_n(t)}, \tag{2.27}$$

where α^n is the polarizability of the individual molecule in the r_n position and the n index runs over the macroscopic ensemble of molecules. According to this expression, the interaction of the electric field with the liquid is defined simply as the sum of single molecule scattering processes. The time dependence of the χ tensor, through the α and r variables, is ruled by the molecular dynamics.

In this equation, there are no hypotheses about the dynamics of the molecules, which is defined by the complete Hamiltonian of the liquid.

To connect the susceptibility tensor with the molecular dynamics, it is useful to separate the intramolecular from the intermolecular dynamics. This separation is applicable when these two dynamics are decoupled.

The intramolecular dynamics is usually described on the basis of vibrational normal modes, $V_v^n(t)$ where n index individuates the molecule and v the vibrational mode. Limiting the mode expansion to the first order, we can write the molecular polarizability as

$$\alpha_{ij}^n(t) \simeq \tilde{\alpha}_{ij}^n(t) + \sum_{n,v} b_{ij}^{n,v}(t) V_v^n(t), \tag{2.28}$$

where $\tilde{\alpha}$ indicates the molecular polarizability with the nuclear configuration at the equilibrium (i.e. rigid molecule approximation), and $b_{ij}^{n,v}(t) = \left[\frac{\partial \alpha_{ij}^n(t)}{\partial V_v^n}\right]$. The expression $\tilde{\alpha}$ can be better defined when the molecule has a polarizability characterized by high symmetry. In particular for symmetric-top molecules (i.e. molecules that have a full axis of rotation) the polarizability can be separated in an isotropic tensor, $\alpha\delta_{ij}$, and a symmetric traceless tensor, $\beta Q_{ij}^n(t)$, [42,44,45]:

$$\tilde{\alpha}_{ij}^n(t) \simeq \alpha\delta_{ij} + \beta Q_{ij}^n(t), \tag{2.29}$$

where α and β are the isotropic and anisotropic part, respectively, of the molecular polarizability. The Q_{ij}^n is the orientational tensor that can be defined as $Q_{ij}^n = (\hat{u}_i\hat{u}_j - \frac{1}{3}\delta_{ij})$, where $\hat{u}$ is the unit vector individuating the molecular axis of symmetry.

In the previous equations, the intramolecular dynamics is defined by the vibrational coordinates, $V_v(t)$, whereas the intermolecular dynamics is contained in several parameters defining the susceptibility tensor. It appears explicitly in the molecule translational coordinates, $r_n(t)$, and implicitly in the rigid-molecule polarizability, $\tilde{\alpha}_{ij}^n$, and mode expansion coefficients, $b_{ij}^{n,v}$. In fact both dependent by the molecule orientational coordinates and hence on the rotational dynamics.

When we introduce the definition of (2.27), (2.28) and (2.29) in the correlation function we get the complete response function measured in any light scattering experiment, apart from the II contributions. This response describes the spectrum from the so called Rayleigh-Brillouin to the Raman roto-vibrational scattering.

In the OKE response only the off-diagonal elements, $i \neq j$, of the dielectric tensor are involved, so the isotropic polarizability, α, does not contribute. Furthermore, the experimental q wave-vector value is zero, hence the translational part of (2.27) is not relevant. Concerning the OKE response the susceptibility tensor definition can be simplified as

$$\chi_{xy}(q,t) \simeq \sum_n \beta Q_{xy}^n(t) + \sum_{n,v} b_{xy}^{n,v}(t) V_v^n(t). \tag{2.30}$$

Using this dielectric tensor in the correlation function (2.24) and supposing no correlation between the vibrational modes of different molecules, we get the following contributions:

$$\begin{aligned}\Phi^{\mathrm{oke}}_{\chi\chi}(t) &= \Phi^{\mathrm{Rot}}(t) + \Phi^{R-V}(t),\\ \Phi^{\mathrm{Rot}}(t) &= \sum_{n,m} \beta^2 \left\langle Q^n_{xy}(t)\, Q^m_{xy}(0) \right\rangle, \qquad (2.31)\\ \Phi^{R-V}(t) &= \sum_{n,v} \left\langle b^{n,v}_{xy}(t) V^n_v(t)\, b^{n,v}_{xy}(0) V^n_v(0) \right\rangle. \qquad (2.32)\end{aligned}$$

The correlation separates into two main parts: one is purely determined by the rotational dynamics, Φ^{Rot}, the other one, $\Phi^{R-V}(t)$, by the intramolecular vibration, V^n_v, modulated by the rotational processes via the $b^{n,v}$ coefficients. Both these two contributions are typically present in the OKE signal.

The $R{-}V$ correlation produces a fast oscillating decay whose relative frequencies and damping rates correspond to the Raman lines [7, 9]. This part of the OKE is sometimes called the Raman-induced Kerr effect [40]. From the experimental point of view, the intensity of the $R{-}V$ is strongly dependent by the laser pulse duration. Typically, short pulses of duration 50 fs or less are able to excite intramolecular vibrations by the Raman-induced Kerr effect since their corresponding bandwidth is large enough to reach the Raman-active vibrations present in the organic molecules.[5] If the pulse is of a longer duration, the effective bandwidth is reduced and the higher frequency dynamics can be cut out so that they do not contribute to the signal [27].

The Rot correlation produces a complex relaxation pattern that has to be addressed to the whole rotational dynamics inclusive of librational and diffusive dynamics. This dynamics has been extensively studied by OKE experiments in simple molecular liquids. For example, the liquid phases of benzene or carbon disulfide are particularly interesting systems. In fact, they can be considered symmetric-top rigid molecules (i.e., the molecular polarizability has a cylindrical symmetry and all the vibrational modes have very high frequencies, not excitable by the laser pulses spectrum). Even in such simple molecular liquids, the interpretation of several dynamics is still open to debate [19, 20, 36] (see also Sect. 2.5.1).

On the basis of 2.31, two different contributions to the correlation can be identified:

$$\begin{aligned}\Phi^{\mathrm{Rot}}(t) &= \Phi^{\mathrm{self}}(t) + \Phi^{\mathrm{cross}}(t),\\ \Phi^{\mathrm{self}}(t) &= \sum_{n} \beta^2 \left\langle Q^n_{xy}(t)\, Q^n_{xy}(0) \right\rangle, \qquad (2.33)\\ \Phi^{\mathrm{cross}}(t) &= \sum_{n\neq m} \beta^2 \left\langle Q^n_{xy}(t)\, Q^m_{xy}(0) \right\rangle, \qquad (2.34)\end{aligned}$$

where Φ^{self} describes the orientational self-correlation of the single molecule and Φ^{cross} the cross-correlation between different molecules.

2.3.1.2 The Mesoscopic Variables

In the previous section we connected the susceptibility tensor directly to the microscopic parameters, the molecular polarizabilities. Indeed, this point of view clarifies the molecular aspects of the χ tensor, but the connection with the dynamical model is complicated by the extremely large number of variables that must be considered. An alternative possibility is represented by a coarse-grained definition of the susceptibility function, in fact if we disregard to the microscopic information we gain a more direct link to the dynamic model. The polarizability of a rigid symmetric-top molecule can be described by (2.29), hence the dielectric tensor becomes

$$\chi_{ij}(q,t) \simeq \sum_n \left[\alpha\delta_{ij}\,\mathrm{e}^{\mathrm{i}q\cdot r_n(t)} + \beta Q^n_{ij}(t)\,\mathrm{e}^{\mathrm{i}q\cdot r_n(t)}\right]. \tag{2.35}$$

It is worth noting that the first term on the right hand side of this equation is time-dependent only through the translational molecular degree of freedom, r_n, since the isotropic part of the polarizability is not dependent on the molecule orientation. This term is directly connected with the microscopic numerical density:

$$\rho(q,t) = \sum_n \mathrm{e}^{\mathrm{i}q\cdot r_n(t)}. \tag{2.36}$$

Conversely the second term is time-dependent through the molecular rotational degree of freedom since the definition of tensor Q^n_{ij} is in the laboratory coordinate, and so in this term there are both the translational and rotational degrees of freedom. We can define the orientational tensor as

$$Q_{ij}(q,t) = \sum_n Q^n_{ij}(t)\,\mathrm{e}^{\mathrm{i}q\cdot r_n(t)}. \tag{2.37}$$

This tensor is clearly determined by the distribution of the molecular axes. Indeed when $q{\sim}0$, as in the specific case of OKE response, this tensor is completely defined by the molecular axis distribution.

To introduce the mesoscopic level in these expressions, we must consider a coarse-graining procedure. This is indeed a nontrivial statistical method that allows averaging of the microscopic functions, previously reported, obtaining a mesoscopic function. Following this approach we can define [48, 49]

$$\tilde{\rho}(q,t) = \langle\rho(q,t)\rangle_{c-g}, \tag{2.38}$$

$$\widetilde{Q_{ij}}(q,t) = \langle Q_{ij}(q,t)\rangle_{c-g}, \tag{2.39}$$

where with the notation $\langle\rangle_{c-g}$ we indicate the partial averaging defined by the coarse-graining procedure. This average is evidently different from the

ensemble average that defines the correlation function. After this coarse-graining average, the microscopic functions become mesoscopic observables where the microscopic information is averaged out. These functions show a smoother space/time dependence and verify the condition of local thermodynamic equilibrium. Hence we can rewrite the susceptibility as

$$\widetilde{\chi_{ij}}(q,t) \simeq \; a\; \tilde{\rho}(q,t)\; \delta_{ij} + \; b\; \widetilde{Q_{ij}}(q,t), \tag{2.40}$$

where a and b are the averaged coefficients derived from the isotropic and anisotropic parts, respectively, of the molecular polarizability [48, 49].

Expression (2.40) is a very useful definition of the susceptibility tensor since it allows a direct link with the hydrodynamic models of complex liquids, as we will show in the next section.

If we focus our attention on the OKE response, only the off-diagonal elements, $i \neq j$, of the susceptibility tensor are involved and the q-dependence can be neglected. So we can simply consider

$$\chi_{ij}(t) \simeq b\; \widetilde{Q_{ij}}(t). \tag{2.41}$$

Hence the relevant correlation function becomes

$$\Phi^{\mathrm{oke}}_{\chi\chi}(t) = \Phi_{QQ}(t) = b^2 \left\langle \widetilde{Q_{xy}}(t)\; \widetilde{Q_{xy}}(0) \right\rangle, \tag{2.42}$$

where only the rotational degrees of freedom are relevant. In contrast to the previous microscopic expressions, (2.31) and (2.32), no intramolecular dynamics is present. Furthermore, since the $\widetilde{Q_{xy}}$ function is mesoscopic, no separation between the $self$ and $cross$ correlation is applicable.

2.3.2 The Model of Liquid Dynamics

The physics of molecular liquids has been described through many different approaches and models, reported widely in the literature. The general framework of the liquid physics can be found in the following references: [50–53], which includes the more recent developments on complex liquids. The basic hydrodynamic point of view of the liquid phase can be found in: [54,55]. Finally the fundamental spectroscopic techniques devoted to the liquid investigations are reported in [42, 56, 57].

Nevertheless, the present physical models on liquid phases are far from reaching a comprehensive picture of the dynamical scenario. Focusing on complex liquids, even the single dynamic process has been, very often, only partially elucidated. Here we recall some of the typically exploited models to describe and to address the relaxation processes measured in an optical scattering experiment, both OKE and LS. According to a simplified scheme, these models can be classified into two main groups.

The first group starts from a microscopic description of the liquid by the molecular variables and usually estimates the equilibrium average of only a few variables on the basis of a proper statistical model. This procedure allows the evaluation of some dynamic parameters of the liquid susceptibility, as introduced previously in the microscopic model. Recently this approach deeply benefits from computer simulations that enable the extraction of a valid molecular picture of the liquid dynamics from the OKE signal [58, 59].

The second series of models is based on the mesoscopic definition of the liquid variables, as introduced in the previous paragraph, and they focus on the collective dynamic processes. Typically the mesoscopic variables, or their correlators, follow few equations of motion derived from the basic conservation laws [42, 54, 55] or the projection procedure introduced in the Mori-Zwanzig theory [42, 52]. The solution of these equations determines the liquid dynamics. Recently these types of models have encountered a renewed interest, thanks to their application to visco-elastic and glassy liquids [48, 49, 60–62].

Here we just want to recall the main characteristics of the theoretical models, of both types, as they have been used in order to describe the relaxation phenomena measured by the OKE experiments. We focus on a few interpretations of the OKE relaxation. One, immediately following, belongs to the first group; the others relate to the second category.

2.3.2.1 Relaxation Processes and Local Vibrations

Historically, a large amount of OKE data on relatively simple molecular liquids have been described according to a basic separation between the fast and the slow dynamics [57]. Indeed, this decoupling of the molecular dynamics is not always appropriate, but it has been and is widely used [20]. In this framework the OKE correlator (see (2.24)) can be divided as

$$\Phi^{\mathrm{oke}}_{\chi\chi}(t) = \Phi^{\mathrm{fast}}(t) + \Phi^{\mathrm{slow}}(t). \tag{2.43}$$

The proper definition of these two correlators is the fundamental issue. Very often the slow correlator is addressed to the orientational self-correlation of the single rigid molecule, see (2.33), which according to the *Debye-Stokes-Einstein model* (DSE) can be described as a pure Brownian diffusive process [19, 42]. Hence the slow correlator becomes

$$\Phi^{\mathrm{slow}}(t) \equiv \Phi^{\mathrm{self}}(t) = \Sigma_n A_n \, \mathrm{e}^{-\frac{t}{\tau_n}}, \tag{2.44}$$

where the number of exponentials and relaxation times, τ_n, are defined by the molecular symmetry. For a true-symmetric-top molecule (i.e., a molecule having a cylindrical symmetry in the diffusion and the polarizability tensors, with coinciding space axis), the $\Phi^{\mathrm{slow}}(t)$ decays as a single exponential characterized

by a relaxation time, called the tumbling orientational time. The relaxation times can be connected to the liquid shear viscosity, η, by the following relation [42]

$$\tau_n = \frac{\eta V_{\text{eff}}}{k_{\text{B}} T} \tag{2.45}$$

where V_{eff} is the effective hydrodynamic volume of the molecule, k_{B} is the Boltzmann constant, and T is the temperature. The definition of V_{eff} is a crucial point of the DSE model and it takes into account, at a very simple and phenomenological level, some of the intermolecular dynamics. To improve the hydrodynamic definition of the (2.45), the V_{eff} has been connected to the real molecular volume, V_{m}, by a multiplicative coefficient, f, being $V_{\text{eff}} = fV_{\text{m}}$. The parameter f defines the boundary condition and it can be calculated on the basis of a geometrical definition of the molecule [19].

Moreover, as shown in (2.33) and (2.34) the OKE signal has a collective contribution even if the sample is approximated as an ensemble of rigid symmetric molecules. Hence a more appropriate approximation for the slow OKE signal should take into account the cross-correlation term: $\Phi^{\text{slow}}(t) \equiv \Phi^{\text{self}}(t) + \Phi^{\text{cross}}(t)$. The evaluation of the cross-term is intrinsically much more complicated than the self-term since it is a many-body function. A possible analysis of such term can be undertaken using the Mori-Zwanzig theory [42,56], where the many-body problem can be reduced to a few "primary/slow" dynamic variables averaging the "secondary/fast" variables. According to this theoretical procedure, Keyes and Kivelson [63] showed that the "collective" rotational correlation function, i.e. $\Phi^{\text{slow}}(t)$, can be approximated again as a single exponential decay with a normalized relaxation time: $\tau_{\text{c}} = \frac{g}{j}\tau_n$, where the g and j factors have a precise statistical definition.

The fast correlator (See (2.43)) describes all the liquid dynamics that is not a pure diffusive process. So, on the fast time scale, the liquid is taken to be in "frozen" structures. The molecules can vibrate/librate but their mean positions are substantially fixed. The fast vibrational/librational dynamics is collective but typically does not show correlation over many molecules, and so it can be studied as a local dynamics. There are no exact models able to describe such many-body problems [57], but there exist different phenomenological approaches. They are a natural progression of the long-standing problem of cage structures in molecular liquids [64].

The interpretation of OKE data based on this reported model has been only partially successful. Indeed, the separation between fast and slow dynamics is often arbitrary [36]. The picture of slow/diffusive processes as a single molecule moving in the surrounding molecules, if acceptable for a massive solute molecule in a solvent of smaller molecules, it is clearly oversimplified for neat liquids [19]. In particular, in complex liquids the important role of collective motion and of cooperative effects for the long time dynamics has been demonstrated

and the single molecule picture appears as an oversimplified one. Also the generalization introduced by Keyes and Kivelson is often not able to reproduce some of the simpler results obtained from OKE experiments, in particular the nonsingle-exponential decay of the signal present in the slow time scale. Furthermore, the interpretation of OKE signal relaxation in the fast/vibrational time scale remains an open issue, even in the simplest molecular liquids [20,36,59].

2.3.2.2 Hydrodynamic Models

Hydrodynamic models have been for a long time utilized to describe the spectrum of light scattering from complex liquids [42], but only recently have they been employed to interpret time-resolved spectroscopic data. As we introduced, this model starts from a mesoscopic definition of the liquid variables. We found that, in order to describe the OKE signal, a single correlator (see 2.42) can be retained. Since the $\widetilde{Q}(t)$ is a coarse-grained variable, its dynamics can be described by the hydrodynamic equations. Indeed only recently has been suggested an hydrodynamic model that takes into account translation/density, $\tilde{\rho}(q,t)$, and rotational variables, $\widetilde{Q_{ij}}(q,t)$, with the proper coupling mechanism [48,49]. In the hydrodynamic model introduced by Pick et al. [49], it is proved that the direct coupling between slow density dynamics and orientation variables can be neglected in the evaluation of OKE response (i.e. in the limit of small q wave-vector). The basic dynamic equation can be written as[6]:

$$\ddot{Q}_{xy}(t) + \int \gamma(t-t')\dot{Q}_{xy}(t')\,\mathrm{d}t' + \omega_{v-l}^2 Q_{xy}(t) = 0, \tag{2.46}$$

where we drop the upper tilde, $\widetilde{\cdot}$, in order to simplify the mathematical notation. This equation enables the evaluation of time evolution of the Q variable, and hence of the OKE response. In fact, as we showed in (2.23), the OKE response function $R_{\mathrm{oke}}(t)$ is defined by the time derivative of the correlation function of the susceptibility that in the present case reduces to the orientational tensor $Q_{xy}(t)$, see (2.42). Alternatively, $R_{\mathrm{oke}}(t)$ can be directly calculated from the dynamic (2.46), through the Green function of this integro-differential expression, $G^{QQ}_{xyxy}(t)$. In fact, we have simply [9] $R_{\mathrm{oke}}(t) \propto G^{QQ}_{xyxy}(t)$.

The dynamic (2.46) is an integro-differential second-order expression where it appears a simple term proportional to Q and a complex term defined by the convolution of the Q time-derivative. The simple term describes a vibrational/librational dynamics summarized in the ω_{v-l} frequency. This dynamical process, similar to the previous "fast" dynamics, could be considered the oscillatory motion of a representative molecule in an effective local harmonic potential well defined by the frozen local liquid structure. The complex term describes the slower dynamical phenomena by means of a memory function, $\gamma(t)$. This function is the key parameter to describe the dynamics of complex liquids. This dynamical equation and the memory function can be also rigorously obtained

from the Mori-Zwanzig theory [42,52]. Depending on the γ-function definition different dynamic phenomena can be included and described by the model. The simplest possibility is the Markovian approximation: $\gamma(t) = \nu\delta(t)$, which transforms (2.46) into the dynamical equation of a simple damped oscillator.

2.3.2.3 Mode-Coupling Models

Alternatively the hydrodynamic equations of motion can determine directly the time evolution of the correlation functions instead of the mesoscopic variables, according to the Mori-Zwanzig model [42,52]. These equations are the starting point of the Mode-Coupling Theories (MCT) [60–62].

In the *schematic model* of MCT [60–62], the dynamic equation of the density correlator, $\Phi_{\rho\rho}(t) = \langle\rho(t)\rho(0)\rangle/\langle\rho^2(0)\rangle$, is taken in the following form:

$$\ddot{\Phi}_{\rho\rho}(t) + \int \mathcal{M}(t-t')\dot{\Phi}_{\rho\rho}(t')\,\mathrm{d}t' + \Omega^2\Phi_{\rho\rho}(t) = 0, \tag{2.47}$$

where the memory function $\mathcal{M}$ has a simple Markovian term, $\eta\delta(t)$, plus a real memory effect that, according to the schematic model, can be represented by a second-order expansion of the density correlator:

$$\mathcal{M}(t) = \eta\delta(t) + A\Phi_{\rho\rho}(t) + B\Phi^2_{\rho\rho}(t). \tag{2.48}$$

So the MCT does not provide an analytical form of the memory function, as other theoretical models do, but it defines a general hierarchical way of building it. Clearly this definition of the memory introduces a self-coupling phenomena in the correlation dynamics. These coupled equations, (2.47) and (2.48), can be solved using a few asymptotic approximations. The solution of these equations provides an analytical description of the density dynamics, called *asymptotic results*.

The schematic MCT model predicts an unattained dynamical arrest of any density fluctuation at a critical temperature T_c. This *critical transition* has been related to the formation of a glassy state. In particular, the MCT model makes specific predictions for the dynamics of the density fluctuations above T_c and it provides a detailed analytical form for the density correlation function.[7] In the vicinity of T_c, the relaxation processes are asymptotically divided into two time scales: a fast/intermediate regime, called β-relaxation process, followed by a long time, or α-relaxation process. In the latter, the correlation function of the density fluctuations decays as a stretched exponential, often named the Kohlrausch-Williams-Watts law [60–62]:

$$\Phi_{\rho\rho}(t) = f\mathrm{e}^{-(t/\tau_\alpha)^\beta}, \tag{2.49}$$

where τ_α is the structural relaxation time, β is the stretching factor, and f is the Debye-Waller coefficient. According to the MCT model, the structural times

are strongly temperature dependent being $\tau_\alpha \propto (T - T_c)^{-\gamma}$, where γ is a critical exponent. In the intermediate time scale, i.e. in the β-regime, the relaxation can be described, as first approximation, by a double power law decay [60–62]:

$$\Phi_{\rho\rho}(t) = f + h_a t^{-a} - h_b t^b, \tag{2.50}$$

the first power law is called critical decay and the second von Schweidler decay. The critical exponents a, b, and γ are linked by the following relation [60–62]:

$$\gamma = (1/2a + 1/2b). \tag{2.51}$$

These predictions represent a complete dynamic scenario that has been investigated by numerous experiments [65]. Indeed, such MCT predictions have been able to describe properly the relaxation processes in supercooled liquids, even if the experimental results locate the MCT critical transition, T_c, at temperatures higher than the thermodynamical glass transition.

The OKE signal is dominated by the orientational dynamics (see (2.42)), hence the direct comparison of OKE response with the schematic model is based on the assumption of a complete similarity between density and rotational dynamics. This assumption seems valid in glass-formers for temperatures higher than the MCT critical transition. So according to this hypothesis, the OKE response function is [24]

$$R_{\mathrm{oke}}(t) \propto -\frac{\partial}{\partial t}\Phi_{\rho\rho}(t), \tag{2.52}$$

$$\alpha\text{-regime}: \quad R_{\mathrm{oke}}(t) \propto (\beta/t)(t/\tau_\alpha)^\beta \, \mathrm{e}^{-(t/\tau_\alpha)^\beta}, \tag{2.53}$$

$$\beta\text{-regime}: \quad R_{\mathrm{oke}}(t) \propto h_a \left[at^{(-a-1)}\right] + h_b \left[bt^{(b-1)}\right]. \tag{2.54}$$

These MCT predictions have been compared with the OKE experiments on glass-formers [24–30, 37]. In these analyses, the authors found that the MCT asymptotic solutions properly reproduce the response relaxation in a large time–temperature range. Nevertheless for temperature $T \leq T_c$, the OKE relaxation shows several dynamic features not predicted by the schematic MCT model [27, 30].

Recently a more appropriate theoretical model has been used in order to describe the OKE data [36, 66]. This MCT model is called the *schematic two-correlator* F_{12} model [67] and it takes into account the rotational dynamics. The model is based on two dynamic equations. The introduced density equation (see (2.47) and (2.48)) represents the "master equation." A second equation, called the "slave equation", defines the rotational motions. This can be written

defining the orientational correlator, $\Phi_{QQ}(t) = \langle Q_{xy}(t)Q_{xy}(0)\rangle / \langle Q_{xy}^2(0)\rangle$, and its memory equation:

$$\ddot{\Phi}_{QQ}(t) + \int m(t-t')\dot{\Phi}_{QQ}(t')\,\mathrm{d}t' + \omega^2\Phi_{QQ}(t) = 0, \tag{2.55}$$

being:

$$m(t) = \nu\delta(t) + C\Phi_{\rho\rho}(t)\Phi_{QQ}(t). \tag{2.56}$$

The density dynamics does not depend by the orientational motion, as evident by (2.47) and (2.48), whereas the orientational dynamics clearly is determined by the density as is shown by (2.56). This translational-rotational coupling is present also when we are considering dynamic phenomena characterized by small or negligible q wave-vectors, different from the direct hydrodynamic coupling reported in [49] that is active only for large values of q.

The solutions of the F_{12} model are normally found by numeric calculations [36,66,67], because there does not exist a simple analytical solution. Only recently, the asymptotic solutions of this model have been calculated [66, 68], providing a relatively simple functional form of the correlation functions.

According to (2.23) and (2.42), the OKE response function is defined by the time derivative of the orientational correlation function:

$$R_{\mathrm{oke}}(t) \propto -\frac{\partial}{\partial t}\Phi_{QQ}(t) \tag{2.57}$$

The comparison of F_{12} model with the OKE data has been performed only in a limited number of cases [36, 66] and it seems able to explain some of the complex relaxation features. We will discuss this shortly in Sects. 2.5.1.2 and 2.5.2.

2.4 The Experimental Procedure

In this section, we will describe the experimental apparatus that is typically utilized in order to perform a heterodyne-detected OKE experiment. In particular we will present the experimental systems developed and assembled in our laboratory.

First of all, a laser source able to produce short pulses with high energy is required. Presently there are a large variety of ultrafast laser systems available on the market. Substantially all these laser systems are based on the Ti:sapphire solid state active medium and on the Kerr lens mode-locking principle. There is a large amount of literature on this subject [69] and we will recall here only the principal features of our present laser system. This is composed of a Kerr lens mode-locked Ti:sapphire oscillator and a chirped pulse amplification system [19, 70], see Fig. 2.2. The oscillator source is a Kerr-lens mode-locked Ti:sapphire laser (FemtoRose 10MDC, by R&D Ultrafast Laser) pumped by

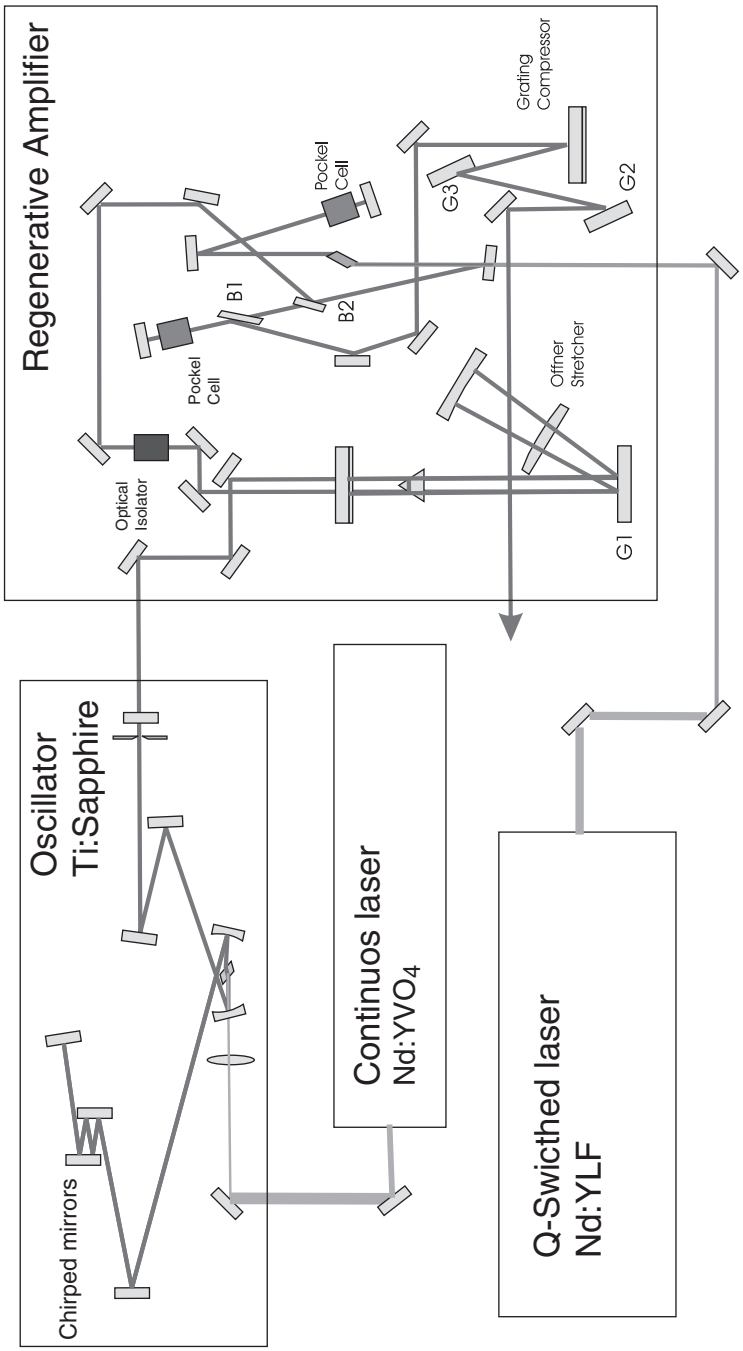

Fig. 2.2 Optical scheme of a typical laser system. Here we report an ultra-fast laser system based on Ti:sapphire solid state active medium and on the Kerr lens mode-locking principle. The main oscillator uses the chirped mirrors technique and the regenerative amplifier is based on a chirped pulse amplification scheme

the second harmonic of a laser-diode-pumped Nd:YVO_4 laser (Millennia V, by Spectra-Physics). Positive dispersion of a 2 mm thick gain medium is compensated by chirped mirrors. The round trip time is 13.7 ns corresponding to a repetition rate of 73 MHz. The minimum pulse width is around 10 fs for the large spectrum cavity operating mode. By a proper choice of the cavity chirped mirror the laser can operate in a narrower spectrum mode, giving a pulse width $\approx$20 fs. The amplification system (Pulsar, by Amplitude Technologies) is based on the chirped pulse amplification technique. The laser pulses from the oscillator are sent to an Offner stretcher and then to a Ti:sapphire regenerative cavity, pumped by a Q-switched Nd:YLF laser (Evolution, by Spectra-Physics). At the end, they are compressed back by a classical, two-grating, compressor design. The amplification stage produces $\approx$0.7 mJ at 1 KHz with a minimum pulse width of about 40 fs. The regenerative cavity includes two Pockel's cells in order to optimize the contrast ratio between main and satellite pulses (5×10^{-7}).

Though there is a most common optical scheme to perform HD-OKE experiments, a few variants are possible [71, 72].

Here we describe our optical set-up that has shown to be particularly successful in order to induce and detect the birefringence dynamics with high energy and low repetition laser pulses [19, 25, 27–29, 36, 37]. In this experimental set-up (see Fig. 2.3) the laser beam is divided into the exciting and the probing beam (about 80%–20%) by a beam splitter, BS1. The exciting pulse arrives

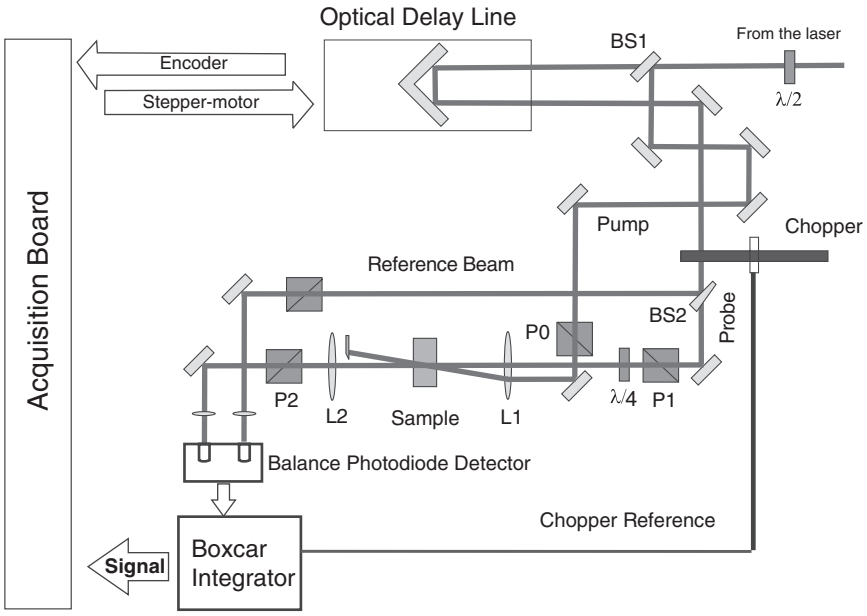

Fig. 2.3 A typical optical set-up and detection scheme used in OKE experiments

directly on the sample, passing through a polarizer P0, that produces a linear polarization along the $\hat{x}$ axis, see also Fig. 2.1. The probing pulse is delayed through an optical delay line, ODL, controlled by a computer. The ODL is made from a specular corner-cube, that produces a safe back reflection of the probe beam, mounted on a motorized stage. Typically, the time resolution of a OKE experiment is not determined by the limitation in optical delay control (easily better then 2–3 fs) but by the laser pulse duration. The probe then is split by a second beam-splitter (BS2) generating the so-called reference beam and finally it arrives at the sample through a polarizer P1 that selects the direction of polarization (45° with respect to the pump beam). Both the E^{ex} and E^{pr} are focused on the sample by a lens L1, typically of 500 mm focal length, which accomplishes the spatial superposition of the two pulses. A polarizer P2, crossed with respect to P1, is placed after the sample in order to select the polarization appropriate for the OKE experiment. To perform heterodyne detection (see next section) the signal field has to be beaten with an other field, called usually the local oscillator, E^{lc}. In this set-up this is obtained using a broad band $\lambda/4$ wave-plate, placed between P1 and the sample. This wave-plate is adjusted to get the minimum leakage out from the P2 polarizer, in the presence of the sample and of L1, then it is rotated by a small angle to generate the local field.

The detection of the signal in HD experiments is not always straightforward. In fact several contributions are simultaneously present on the detector, see next section, and the disentanglement of them is required. In our experiment we used a differential photodiodes system: one photodiode measures all the electromagnetic fields coming from the sample, $\mathbf{E}^{\mathrm{sg}} + \mathbf{E}^{\mathrm{lc}}$, the other photodiode is balanced with the reference beam to compensate for the intensity of the local field. The output of the differential is set to zero, in absence of the excitation beam. A boxcar gated integrator, synchronized to a mechanical chopper placed on the exciting beam, collects the output of the differential photodiode amplifier allowing an automatic subtraction of the other backgrounds present in the signal. The signal is at the end recorded by an acquisition board, which also controls and measures the position of the optical delay line. The homodyne contribution is eliminated by subtracting two different measurements taken with opposite direction of the rotation of the $\lambda/4$ plate. In fact, these two measurements are characterized by a positive terms for S_{homo} and by the S_{hete} signal with opposite signs, see (2.63).

The HD-OKE data are composed by a number of time-points corresponding to different positions of the optical delay line. When a step-by-step acquisition procedure [19] is used, the optical delay line moves one step and stops waiting for the signal acquisition. Typically the data have about few thousand of time-points. For each time-point the signal intensity is the average over few hundreds of laser pulses. If a very wide experimental time window is needed we perform

separated scans of the delay line, characterized by a series of time-points spaced with different steps (e.g. from 0 ps to 4 ps we use a time-step of 5 fs, from 2 ps to 18 ps we use a time-step of 10 fs and for the remaining time window a logarithmic time-step). Then these scans are matched to rebuilt a single datafile, using an extreme attention to the signal consistency in the overlapping time regions.

We found extremely useful to perform each scan with optimized laser pulses [28, 37]. Typically pulses of different energy and temporal length are utilized to optimize the signal-noise ratio e.g., excitation pulses of 50 fs and 1.2 μJ (transform-limited) are employed in the short scan and excitation pulses of 1 ps and 12 μJ (chirped) in the long scan. With longer laser pulses, it is possible to transfer a larger quantity of energy to the system without increasing the instantaneous intensity of the pulse. The signal is then characterized by a better signal–noise ratio that allows access to a longer temporal scale. Using the heterodyne detection and stretched pulses more than five intensity decades can be scanned (see Fig. 2.4).

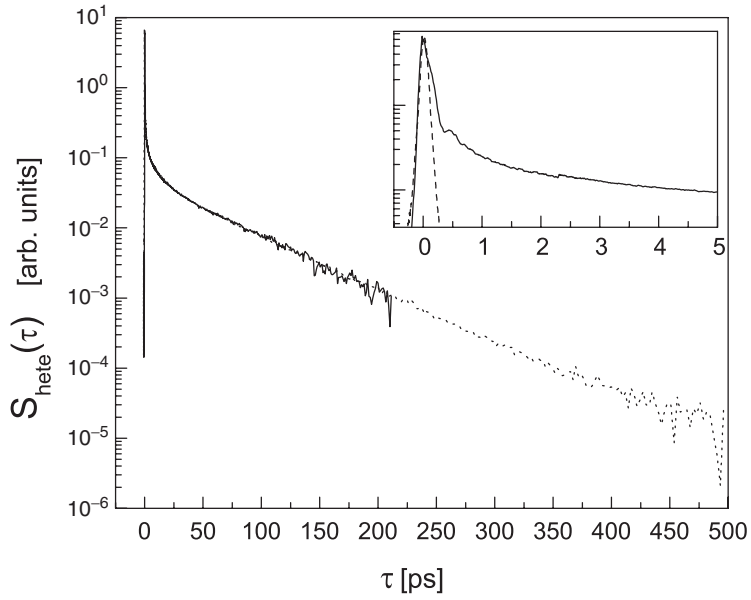

Fig. 2.4 The signal measured in a HD-OKE experiment on a epoxy resin (phenyl glycidyl ether) [28]. We show the OKE data obtained with laser pulses of different durations. In the long scan (dotted line) we used laser pulses of 1 ps, in the short scan (continuous line) the pulses were of 50 fs. In the inset figure, we show the same data in a very short time window. The dashed line is the instrumental response, obtained performing the OKE experiment on a sample with only instantaneous response, typically a quartz plate

2.4.1 Heterodyne Detection

In the heterodyne detection scheme, the signal, $\mathbf{E}^{\rm sg}$ defined in (2.21), interferes with an extra field, called local field $\mathbf{E}^{\rm lc}$, on the detector. The integrated intensity, measured by the main photodiode D1 in our set-up, is then

$$\begin{aligned} S_{\rm tot} &\propto \int {\rm d}t\, |\mathbf{E}^{\rm sg}(t) + \mathbf{E}^{\rm lc}(t)|^2 \\ &= \int {\rm d}t\, \left\{ |\mathbf{E}^{\rm lc}(t)|^2 + |\mathbf{E}^{\rm sg}(t)|^2 + 2{\rm Re}[\mathbf{E}^{\rm sg}(t)\cdot\mathbf{E}^{\rm lc}(t)^*] \right\}. \end{aligned} \tag{2.58}$$

There are three contributions in the previous equation: the first is the intensity of the local field, the second is the homodyne signal, see also (2.9), and the third one is the heterodyne signal

$$\begin{aligned} S_{\rm lc} &\propto \int {\rm d}t\, |\mathbf{E}^{\rm lc}(t)|^2, \\ S_{\rm homo} &\propto \int {\rm d}t\, |\mathbf{E}^{\rm sg}(t)|^2, \\ S_{\rm hete} &\propto \int {\rm d}t\, 2{\rm Re}\left\{ \mathbf{E}^{\rm sg}(t)\cdot[\mathbf{E}^{\rm lc}(t)]^* \right\}. \end{aligned} \tag{2.59}$$

Of course, in a HD-OKE experiment the relevant signal is the last one, the others are contributions to be eliminated. As we already mentioned, the $S_{\rm lc}$ signal can be read out with the differential photodiode detector. This is a fundamental experimental device and it allows us to clean up a strong contribution in the total signal, typically $S_{\rm lc}/S_{\rm hete} \sim 10{-}100$, which otherwise would seriously restrict the dynamic range of the detector. Furthermore, using as reference a part of the probe beam, the eventual effects of the slow drifts or fluctuations in the laser intensity are reduced. As we showed in the previous Sect. 2.2.1, the $S_{\rm homo}$ is indeed a signal that contains all the dynamical information (see (2.9)) but it is connected to the squared response. When the response has a complex relaxation pattern, this squared terms makes it even more difficult to address the different dynamic modes. So the $S_{\rm homo}$ contribution is considered a kind of spurious effect in the signal detection that has to be subtracted. This is possible because it does not dependent on the $\mathbf{E}^{\rm lc}$ and it can be subtracted performing two measurements characterized by opposite phase of the local field (i.e. π out-of-phase).

In our experimental set-up, the local field is generated by rotating the $\lambda/4$ plate of a small angle, ε. This wave-plate rotation produces a leakage of the probe beam from the P2 polarizer that represents our local field. This is proportional to the probe field and it can be calculated using the Jones matrix algebra [73]:

$$\mathbf{E}^{\rm lc} = (\hat{\rm e}_x - \hat{\rm e}_y)\eta\, E^{\rm pr} \text{ with } \eta = \varepsilon + {\rm i}\varepsilon, \tag{2.60}$$

where ε is the angle formed between the fast axis of the wave-plate and the polarization direction selected by the polarizer of analysis, P2. Typically this is

a small angle of few degrees and it can be positive or negative. The local field, so obtained, is a valid local field because it has an easily variable intensity and it is locked in phase with the signal field. If the local field is obtained by the wave-plate rotation the local field has a mixed phase (i.e. it contains in-phase and out-of-phase components) compared to the signal field, as is shown by (2.60). We can produce a local field also by rotating the P1 or the P2 polarizers. In such a case the local field has a well defined phase: the P1 rotation produces a $\pi/2$ out-of-phase field (i.e., $\eta = \mathrm{i}\varepsilon$) and the P2 rotation produces a in-phase field (i.e., $\eta = \varepsilon$). As we described previously (see Sect. 2.2.2) if resonant effects are present, the induced polarization, and hence the signal field, has a different phase from the probe field. Considering that $E^{\mathrm{sg}} \propto \mathrm{i}P^3$, the part of the E^{sg} field that is in-phase with E^{pr} defines the dichroic effect, whereas the part that is $\pi/2$ out-of-phase describes the birefringence. So according to the definition of S_{hete} (see (2.59)) by rotating the P1 polarizer, we select the birefringence contribution and by rotating the P2 polarizer we select the dichroic. So, in principle, the creation of a local filed using the P1 and P2 polarizers has the advantage of a clear separation between birefringence and dichroic contributions. Indeed, we adopted this procedure for a direct experimental check of the presence of dichroic contribution in the OKE signal. Unfortunately, from the experimental point of view, any rotation of the polarizers produces a relevant optical misalignment, which makes this method complicated and not always reliable. For this reason is preferable to use the $\lambda/4$ wave-plate, which does not produce any modification of the optical alignment during its rotation.

As we have shown in (2.60), in our experimental procedure the local field has a mixed phase. So, if the response function has any resonances with the laser fields, the signal will have both birefringent and dichroic contributions, whereas in a nonresonant case (as we will consider in the derivation of (2.62)), the signal is determined only by the birefringence effect, even if a mixed phase is present in the local field. Indeed in our nonresonant experiments, we always found the dichroic signal absent or negligible.

According to the definition of the signal field, (2.21) and the local field expression (2.60), the heterodyne signal becomes

$$S_{\mathrm{hete}}(\tau) \propto 2\mathrm{Re}\left\{\mathrm{i}(\varepsilon - \mathrm{i}\varepsilon)\int \mathrm{d}t\, E^{\mathrm{pr}}(t)E^{\mathrm{pr}}(t)^* \int \mathrm{d}t' R_{\mathrm{oke}}(t-t')[E^{\mathrm{ex}}(t')]^2\right\}. \tag{2.61}$$

Since we are considering an OKE experiment the response function is a real number and this equation can be further simplified:

$$S_{\mathrm{hete}}(\tau) \propto \varepsilon \int \mathrm{d}t\, [\mathcal{E}(t-\tau)]^2 \int \mathrm{d}t' R_{\mathrm{oke}}(t-t')[\mathcal{E}^{\mathrm{ex}}(t')]^2, \tag{2.62}$$

where we also introduced the definition of laser pulse envelope, (2.A.6), and the relative intensity expressions, according to (2.A.2). The derived equation

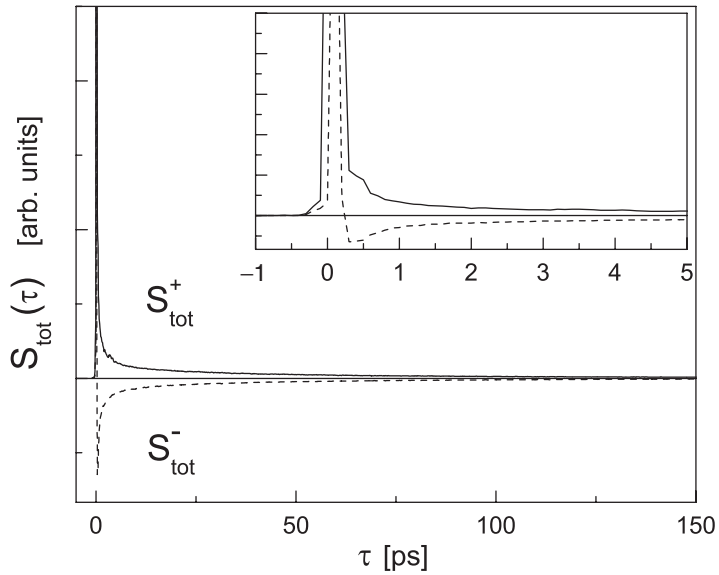

Fig. 2.5 HD-OKE experiment on glass-former m-toluidine at 273 K [25]. We show here the two measured signals $S^{+}_{\rm tot}(\tau)$ and $S^{-}_{\rm tot}(\tau)$ corresponding at two $\pm\varepsilon$ opposite values of the rotation angle of the wave-plate

shows how the heterodyne signal has a sign that depends on the angle ε defined by the wave-plate rotation, so that $S_{\rm hete}$ is positive or negative if ε is positive or negative. However the $S_{\rm homo}$ is always positive. By performing two measurements with opposite values of the angle $\pm\varepsilon$, we will get two opposite signal, $S^{+}_{\rm tot}$ and $S^{-}_{\rm tot}$; it is immediately clear that we can extract from these total signals the heterodyne component:

$$\frac{1}{2}[S^{+}_{\rm tot}(\tau) - S^{-}_{\rm tot}(\tau)] \propto S_{\rm hete}(\tau). \tag{2.63}$$

Performing this subtraction we disentangle the heterodyne signal from the homodyne contribution and, furthermore, we clean up the signal from all the other spurious effects that are not sensitive to the phase of the local field. In Fig. 2.5 we report an experimental example of this procedure.

2.4.1.1 Recent Up-Grading

Recently we introduced an innovative acquisition system for HD-OKE spectroscopy [70]. It is based on a real-time acquisition of the experimental signal during the rapid scan of the optical delay line. This acquisition scheme enables data acquisition with high absolute time resolution (1 fs), high scanning velocity (2.5 cm s^{-1}) and long time delay (several ns). Moreover it is suitable

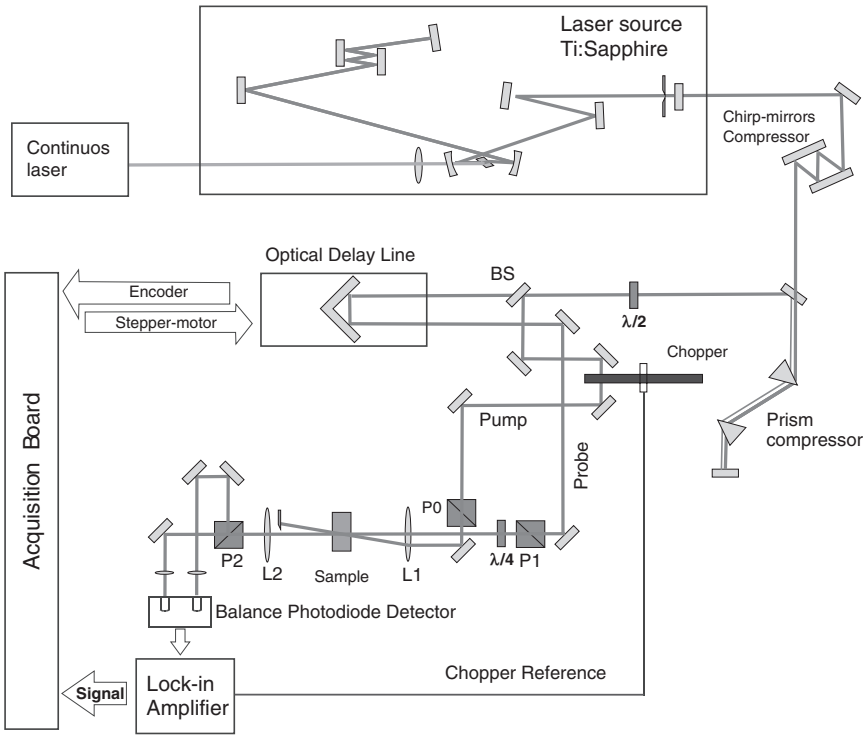

Fig. 2.6 New experimental set-up for HD-OKE spectroscopy with high repetition laser source and real-time data acquisition

for HD-OKE experiments performed with high and low repetition rate laser sources.

In Fig. 2.6 we report the experimental sketch of a HD-OKE experiment, recently built in our laboratory, employing the oscillator as laser source and the aforementioned acquisition system. The optical set-up is identical to that previously reported, apart from an additional optical compressor stage. The pulse compression is realized by the multireflection on two chirped mirrors and the passage through a pair of silica prisms. The background subtraction is obtained using a fast balanced photodiode detector and filtering the signal with a lock-in amplifier. In the real-time acquisition procedure, the delay line moves continuously and the signal is simultaneously acquired, while the delay line position is measured reading the encoder output. Such a system substantially decreases the acquisition time of each single delay scan, improving substantially the signal statistics.

Furthermore, we used the optical set-up in a different way [71]. In this scheme, the $\lambda/4$ wave-plate is rotated in order to produce a circularly polarized

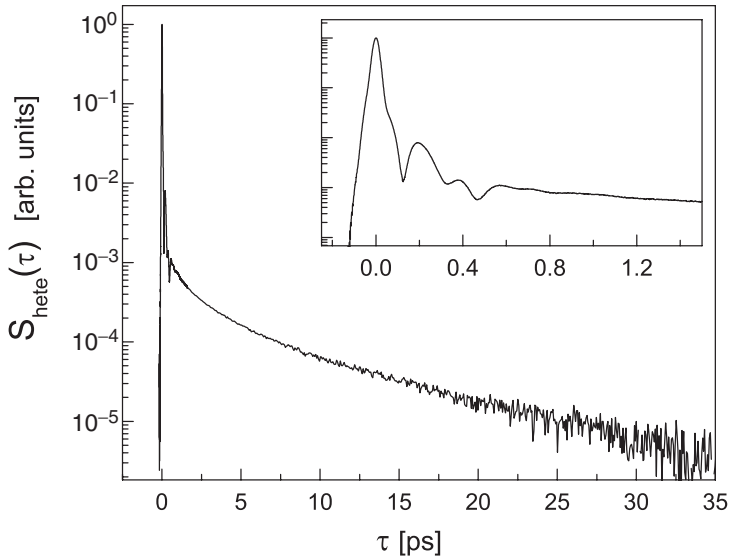

Fig. 2.7 HD-OKE signal on water at 249 K from the new experimental set-up

probe field and the two signals, corresponding to the horizontal and vertical linear polarizations generated by P2, are sent to the balanced photodiode detector. In such a way, an automatic heterodyne of the OKE signal is produced. A further reduction of the noise in the data can be obtained by performing a super-heterodyning of the OKE signal [72]. This is achieved by performing two OKE measurements, corresponding at left and right circular polarizations of the probe field, and making the difference of these two data.

In Fig. 2.7 we report HD-OKE signal on water obtained with this new experimental set-up and technique. Water has a very low OKE signal and it is a particularly difficult sample. Usually it requires quite a complex procedure to be properly investigated with the step-by-step acquisition [37]. With the real-time acquisition it is possible to get a very good signal/noise ratio with an extended dynamic range performing a single and continuous scan of the optical delay line without pulse energy/duration adjustments.

2.4.2 HD-OKE vs. Light Scattering Signal

The HD-OKE signal is directly connected with the response function (see (2.62)); in fact they are coincident when the laser pulse duration is much shorter than the dynamic time scale present in the response function (see (2.12)). Furthermore, the response function is defined by the time-derivative of the correlation function of the dielectric tensor (see (2.23)). These relationships permit the connection of the HD-OKE signal with that measured in a forward

(i.e. the value of $q \sim 0$) depolarized light scattering experiment (DLS). In fact, a DLS experiment measures the spectral density of the dielectric tensor fluctuations [42], that according to the fluctuation-dissipation theorem can be defined as [43, 74]

$$S_{\rm dls}(\Delta\omega) \propto [n(\Delta\omega)+1]\; Im\chi_{\rm dls}(\Delta\omega), \tag{2.64}$$

where $\Delta\omega$ is the frequency difference between the incident and the scattered light, $n(\Delta\omega)$ is the occupation number, and $[n(\Delta\omega)+1] = (1-{\rm e}^{-\frac{\hbar\Delta\omega}{K_{\rm B}T}})^{-1} \simeq \frac{K_{\rm B}T}{\hbar\Delta\omega}$ is the so-called Bose factor. $\chi_{\rm ls}(\Delta\omega)$ is the DLS frequency-dependent susceptibility corresponding to the Fourier transform of the time-dependent response function:

$$\chi_{\rm dls}(\Delta\omega) = \int {\rm e}^{{\rm i}\Delta\omega t}\; R_{\rm oke}(t)\,{\rm d}t. \tag{2.65}$$

Equations (2.64) and (2.65) show directly the connection between the OKE response function and the DLS susceptibility. So finally, we can easily connect the DLS and OKE signals:

$$S_{\rm dls}(\Delta\omega) \propto [n(\Delta\omega)+1]\; Im \int {\rm e}^{{\rm i}\Delta\omega t}\; S^{\rm hete}_{\rm oke}(t)\,{\rm d}t. \tag{2.66}$$

This relation has been also checked experimentally [74, 75].

2.5 Some Experimental Results

There is a large amount of literature on OKE results, as we summarized in the introduction. A complete review of this literature is beyond the aim of this section. We simply summarize some of our OKE results on different complex liquids, trying to give a general scenario of the liquid dynamics as measured by OKE experiments. Furthermore, we do not discuss the vibrational part of the dynamics, which has been extensively reviewed in the first chapter. The OKE data reported in this section has been already published or will be shortly, and so we are here just recalling the more relevant aspects. For the details we refer to the published papers.

We divided the data of relative simple liquids, as benzene [36] and iodobenzene [19], from the more complex liquid data, as super-cooled and glass-formers [25, 27]. A special attention is finally devoted to the dynamics of water [37].

2.5.1 HD-OKE in "Simple" Molecular Liquids

The liquid phase formed of small molecules (e.g. CS_2 and C_6H_6) has been largely studied by many OKE experiments [7,8,10,13,18–20,36] and numerical investigations [46,47,58,59]. Despite the relatively simple molecular structure, the dynamics of these liquids still present unclear aspects [20, 36, 59].

2.5.1.1 The Dynamics of Liquid Iodobenzene vs. Debye-Stokes-Einstein Model

As we already introduced in Sect. 2.3.2.1, the slower dynamics of simple liquids has been often described on the basis of the Debye-Stokes-Einstein (DSE) diffusion model. In our paper, Bartolini et al. [19], we checked such model on the dynamics of liquid iodobenzene as measured by HD-OKE experiments.

Actually, the interpretation based on such a single molecule picture appears as an oversimplified one. First of all, the observable in OKE experiments (as well as in a light scattering measurement) is collective in nature. On the other hand, the important role of collective motion and of cooperative effects has been demonstrated for the long time dynamics in several liquids characterized by strong anisotropic interactions. The importance of collective dynamics and of intermolecular interactions is also obvious in the short time limit: The picture of a single molecule librating in the potential well made up by the surrounding molecules, if acceptable for a "slow" solute in a "fast" solvent, is clearly oversimplified for neat liquids. In particular, it completely misses the key point of the correlated dynamics of neighboring molecules, which instead is of fundamental importance to understand the mechanism of liquid dynamics.

In Bartolini et al. [19] we presented the results of HD-OKE experiments performed on liquid iodobenzene in a wide temperature range. The experimental procedure employed in this work has been described in Sect. 2.4; other details can be found in the paper.

A typical long scan of the HD-OKE signal is shown in Fig. 2.8. At least three different time regimes can be distinguished in the relaxation pattern: (1) a long time scale, characterized by an exponential decay, with a time constant ranging between 10 and 20 ps, depending on the temperature; (2) an intermediate range, where the relaxation is quasi-exponential; and (3) the short time dynamics, appearing and lasting for a few picoseconds, showing a well-pronounced fast oscillations together with the early part of the relaxation process. Here we summarize the analysis of the slow and intermediate parts of the OKE signal, while the analysis of the faster dynamics can be found in the paper. According to the model introduced in Sect. 2.3.2.1, the slow and intermediate dynamics have been ascribed to rotational diffusion processes. A first attempt in order to extract the relaxation times present in the signal is the subtraction procedure. For the iodobenzene signal this is shown in Fig. 2.9.

The previous decomposition of the data relaxation suggests a double exponential form of the OKE response function and hence of the related correlator, $\Phi^{\mathrm{oke}}(\tau) = A_1 \, \mathrm{e}^{-\frac{\tau}{\tau_1}} + A_2 \, \mathrm{e}^{-\frac{\tau}{\tau_2}}$. The two relaxation times, τ_1 and τ_2, are compatible with the DSE picture. As reported before, the diffusive relaxation is in general described by a multiexponential decay [42], which for an asymmetric rotator reduces to a biexponential if the principal axes of the rotational diffusion

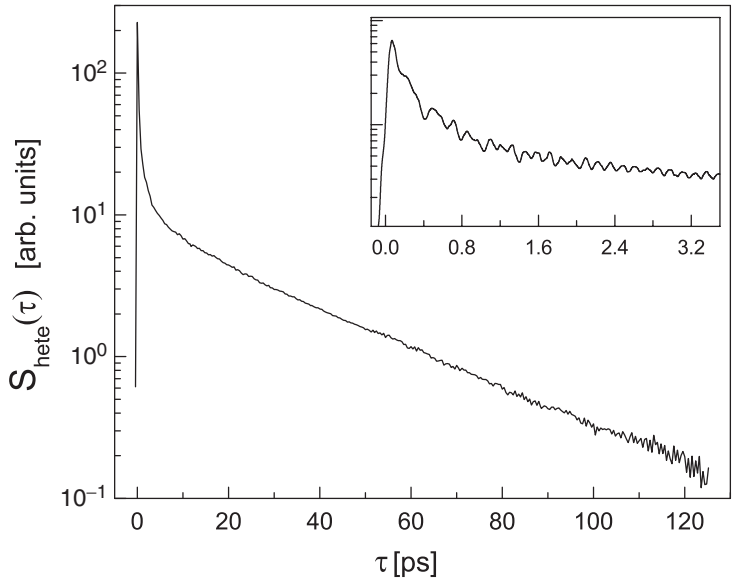

Fig. 2.8 HD-OKE signal from iodo-benzene sample at 273 K. In the inset we show the fast relaxation time scale, where several signal oscillations take place

tensor and of the molecular polarizability coincide. In the DSE model, as shown in (2.45), these relaxation times can be calculated using the shear viscosity, η, the molecular volume, $V_{\rm m}$, and the parameter f. This last parameter depends on the hydrodynamic boundary conditions, slip or stick, and on the shape of the molecule.

The viscosity/temperature dependence of the τ_1 time constant, obtained from the fit of OKE data on iodobenzene, is in substantial agreement with the DSE model for a symmetric rotator within the slip condition. The slower time constant τ_1 coincides with the tumbling motion around the short molecular axis. This result is common to several molecular liquid dynamics. On the other hand, τ_2 is poorly reproduced by the DSE model. In fact if a prolate ellipsoid shape is assumed for iodobenzene, a symmetric rotator, τ_2 contains contributions from both spinning and tumbling reorientations characterized by time values much longer than those measured. If a more complete DSE model based on a asymmetric rotator is used to address the two relaxation times, the situation does not improve. Again τ_1 is correctly calculated but values of τ_2 are completely missed. In the faster time scale of the τ_2 relaxation the molecular motion is affected by the details of the short living local structure to a much larger extent, in comparison to the slower τ_1 dynamics, which instead is determined by interactions averaged over a much longer time.

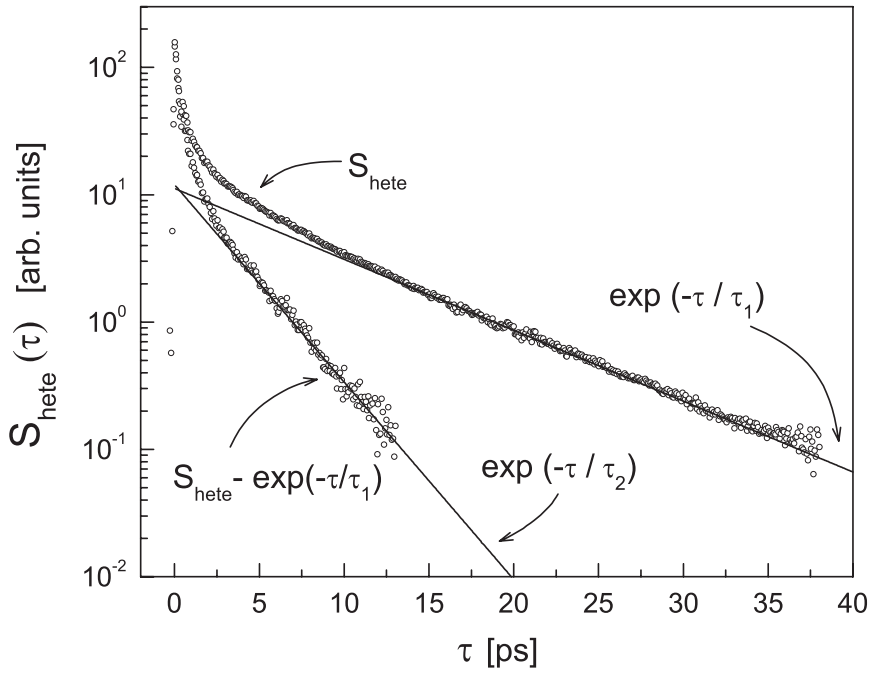

Fig. 2.9 The long part of HD-OKE signal, at 371 K, is well fitted by a single exponential decay of about 7 ps. If we subtract the long decay from the signal a second quasi-exponential decay appears characterized by a ≈2 ps relaxation time

This behavior is very similar to what was observed in other molecular liquids. These results on liquid iodobenzene, together with the other similar studies, pointed out clearly two aspects. Indeed the simple DSE model is able to describe quantitatively the slow relaxation processes. On the other hand, it is not able to properly address other simple dynamical features as the intermediate quasi-exponential relaxation. In our opinion, the DSE is really too simple an approach and the agreement observed for the slower relaxation could be partially fortuitous. Furthermore the starting hypothesis of decoupling of fast and slow dynamics does not have any safe physical background.

2.5.1.2 The Dynamics of Liquids Benzene vs. Mode-Coupling Theory

The dynamics of many molecular liquids, characterized by a simple molecular structure, show similar features. As we reported in the case of liquid iodobenzene, the experimental decays demonstrate the presence of three main time scales: (1) A *fast time scale* (typically up to a few picoseconds) where the driving processes are the intramolecular vibrations; the intermolecular dynamics on this time scale also have a vibrational character. In fact, on the short time scale the

molecules are vibrating around their equilibrium position since it should be a valid approximation to take the liquid structure as static. (2) An *intermediate time scale* (typically some picoseconds) where the liquid structure cannot be taken as static since the diffusion processes start to be effective, producing a structural redefinition. On this time scale the intermolecular vibrations couple strongly with the structural relaxation rearrangement. (3) Finally, the *slow time scale* (whose range strongly depends on the liquid viscosity, varying from 10^{-11} to 10^{-9} s) where the leading effect is the structural relaxation. These recurrent features suggest a possible common dynamic scenario for molecular liquids. The DSE model has been largely utilized to address the slow relaxation. Indeed the apparent quantitative agreement with the data made this approach very popular even if its starting hypotheses are not physically accurate. The fast dynamics, intrinsically vibrational, has been described by many different models (e.g. the Kubo model of stochastic oscillators) with some success. However the nature of the intermediate relaxation remains obscure.

In Ricci et al. [36], we presented a study of the relaxation processes of the liquid and super-cooled benzene by HD-OKE spectroscopy. We have chosen benzene, consisting of perfectly symmetric molecules, as a particularly simple and meaningful example. The time-resolved optical Kerr effect data on benzene are obtained in a large temperature range, including the supercooled state (we succeeded in supercooling benzene by about 20 K below the melting point T_{m} = 279 K). Benzene is a highly symmetric molecule with a stiff molecular structure that does not present intramolecular dynamic contributions to the accessible OKE time scales. Thus it has proved to be an excellent model of a simple molecular liquid. The experimental results have been compared with the two-correlator F_{12} MCT model, see Sect. 2.3.2.3.

Our data [36] confirms and extends to the supercooled phase the results reported in the literature [15, 20]. The dynamics of benzene (see Fig. 2.10) shows three different processes: at very short delays (0.1–1 ps), there is evidence of an oscillatory behavior of the signal, superimposed as a fast quasi-exponential decay. No intramolecular vibration of benzene is low enough to be directly excited within the pulse bandwidth [27]; the origin of the oscillation is then to be found in the intermolecular vibrations. This oscillating signal is followed by a residual intermediate decay taking place up to 4–5 ps. Finally, the slow relaxation process appears and it extends, for the lower-temperature data, up to 40 ps. In several literature reports, the benzene slow dynamics has been attributed to the single molecule orientational diffusion process and it has been analyzed using the DSE model, similarly to our analysis of liquid iodobenzene previously reported. The fast and intermediate dynamics are more complex phenomena that still do not find an agreed interpretation [58, 59]. It has been compared with different models usually based on the local intermolecular vibrations, whose definition is generally quite arbitrary. According to these studies,

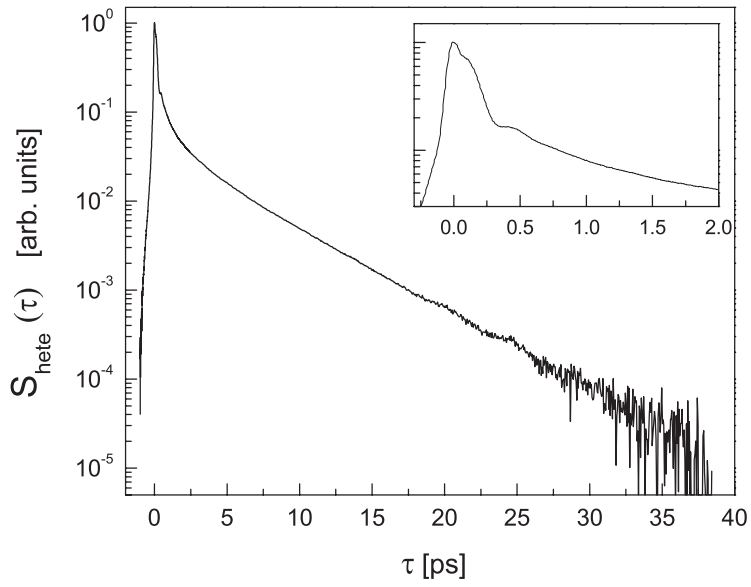

Fig. 2.10 HD-OKE signal from supercooled benzene sample at 269 K, about 10° below the melting point. In the inset we show the fast relaxation time scale, where a smooth signal oscillations take place

two main groups of vibrational modes are present: the first group is made up of under-damped modes characterized by an approximate frequency of 1.2 THz and the second group consists of over-damped modes of about 360 GHz. The first modes describe the fast vibrational dynamics; the second modes reproduce the intermediate relaxation processes. These models require a substantial decoupling between the slow/diffusive dynamics and the fast-intermediate processes. Such a hypothesis is in many respects an oversimplification of the dynamic problem that hardly applies to a molecular liquid such as benzene where all the dynamic features are characterized by similar time scales. Thus a definite assignment of the measured decay has not been worked out. In particular, the nature of the intermediate relaxation remains obscure. Since these dynamic features are repeated and common to many molecular liquids, the open questions are particularly relevant.

We investigated MCT as a possible valid model to describe the dynamics of the molecular liquids. Indeed, MCT models have been able to describe the relaxation features of several glass-formers up to temperatures well above the critical temperature [24, 25, 27–29, 37]. This suggests that the MCT should be tested as a possible model for the dynamics of molecular liquids, even if they do not show a glass transition and are characterized by rather low viscosities. We utilized the schematic two-correlator F_{12} MCT model in order to describe

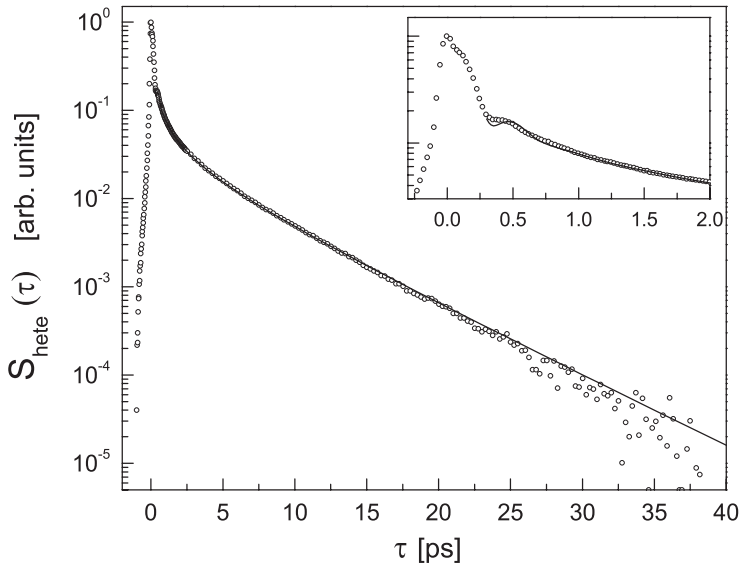

Fig. 2.11 The HD-OKE signal, at 269 K, is well fitted by MCT model up to ≈0.5 ps time

the OKE signal on benzene. The integro-differential equations of the model, reported in Sect. 2.3.2.3, have been solved numerically adjusting the A, B, C, Ω, and ω parameters thorough a fitting procedure in order to optimize the time derivative of the orientational correlator (see (2.57)) to the measured data. A typical fit is reported in Fig. 2.11.

The numerical solution of this model is indeed able to properly fit the benzene decay in the whole relaxation time scale, from about 0.5 to 35 ps. What is striking is the ability to fit the fast, intermediate and slow dynamics without any arbitrary separation of the time scales and of the dynamic processes.

In this MCT model, all the dynamic processes are intrinsically included and coupled. The fast vibration, the slow structural relaxation, and the intermediate decay appear as solutions of the equations of motion. The vibrational dynamics is characterized by two frequency parameters, Ω and ω, of about 1 THz, in reasonable agreement with the mean frequency of the vibrational modes found in previous studies. The crossover from the fast to the slow processes correctly describes the intermediate relaxation. This model does not require extra over-damped vibrational modes, as required by the previous interpretations. According to this interpretation, the intermediate relaxation is simply the merging of the local vibrational dynamics into the slow collective diffusive process. This merging is not trivial, as it has already been proved in glass-former liquids, because the two processes are strongly coupled.

In our opinion, the MCT interpretation represents a valid physical model for the molecular liquids, as here shown for the benzene liquid, and for glass-formers, as we are going to show in the next section.

2.5.2 HD-OKE in Supercooled Liquids and Glass-Formers

Recently the OKE experiments have been shown to be a particularly useful spectroscopic tool to investigate glass-former dynamics [24–30]. Indeed the OKE data enabled a better check of the theoretical models, especially of MCT approaches. In this Section, we summarize the studies of the m-toluidine glass-former performed by the authors [25, 27] as a particularly meaningful example.

Meta-toluidine (CH_3–C_6H_4–NH_2) is a disubstituted benzene ring with CH_3 and NH_2 groups in the 1, 3 positions; it is one of the simplest fragile liquids, which remains very easily supercooled to its thermodynamic glass transition temperature T_g = 187 K, while the melting temperature is $T_\mathrm{m} = 243.5$ K. Starting with 99% pure m-toluidine purchased from Merck, the sample was purified by distillation under vacuum and then kept in a quartz cell. The cell was placed in a cryostat system, cooled with Peltier cells; this enabled temperature control to better than 0.1 K. Our HD-OKE measurements were performed at 15 temperatures between 295 and 225 K with the experimental equipment and laser system, presented in Sect. 2.4. Let us simply recall here that the time resolution allows us to measure the response function by a step-by-step procedure, up to approximately 4 ns. The amplitude of the HD-OKE signal may be detected over a dynamic range of approximately five decades and exhibits a complex relaxation pattern.

In Fig. 2.12 we show HD-OKE signal data on a log–log scale. Each datum is an average of five independent measurements. The measured dynamics exhibit three different regimes: a nearly temperature-independent region from 0.1 to 2–3 ps, where oscillations related to intramolecular vibrations appear; an intermediate decay region from 2 to about 10 ps, depending on the temperature; and the final long-time relaxation. The long-time dynamics have a stretched-exponential form with decay times increasing with decreasing temperature. All the data sets have the same general form, but these major features (the three regimes) occur on different time scales depending on the temperature.

In the supercooled phases of glass-former liquids, the rotational dynamics is expected to be strongly coupled with the density dynamics. Therefore, the orientational and translational dynamics should present similar features. This sensible hypothesis has been verified by several numerical and experimental results [65]. In this framework, it is worthwhile to compare the OKE data on rotational dynamics to the predictions of the schematic MCT model on density dynamics. This comparison is particularly meaningful because the

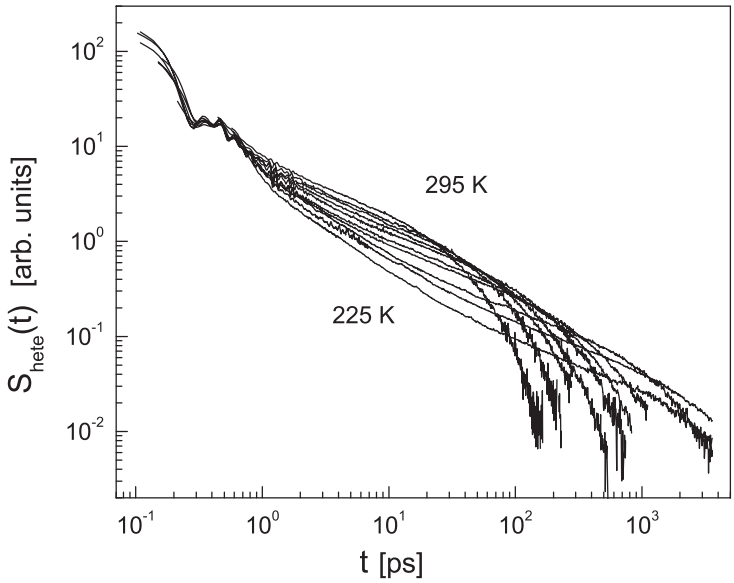

Fig. 2.12 The HD-OKE signal from liquid and supercooled m-toluidine sample. We report the data in a log–log plot in order to show clearly the different time scales present in the relaxation process

asymptotic results, introduced in Sect. 2.3.2.3, define a clear and not trivial dynamical scenario.

Indeed, the MCT asymptotic results have shown to describe successfully the relaxation of glass-formers for relatively weak supercooling condition [65] (i.e. for relatively high temperature, $T \geq T_c$). Whereas for deep supercooling condition (i.e. $T \leq T_c$) the MCT asymptotic results are not applicable, since they predict a structural arrest at the critical temperature (i.e. $\tau_\alpha \rightarrow \infty$ when $T \rightarrow T_c$), which is not experimentally verified in glass-formers. Therefore, more complex MCT models must be used in order to reproduce the experimental results. The OKE experimental results have proved to be a critical check for the asymptotic MCT predictions [24–30]. In particular, we analyzed the intermediate and slow relaxation of OKE signal on m-toluidine according to the asymptotic solution of the schematic MCT model [25]. The fast dynamics has been partially compared with more complex MCT approaches, as the two-correlator F_{12} model [27]. Here we report only the study of the slower relaxation processes.

As shown in Sect. 2.3.2.3, the schematic MCT model can be solved using a few asymptotic approximations [60–62], providing a relatively simple analytical expression for the measured response function (see (2.53) and (2.53)). According to these equations, the analysis of the slow relaxation vs. α-regime can be based on a master plotting technique. In fact, following (2.53) all α-correlation

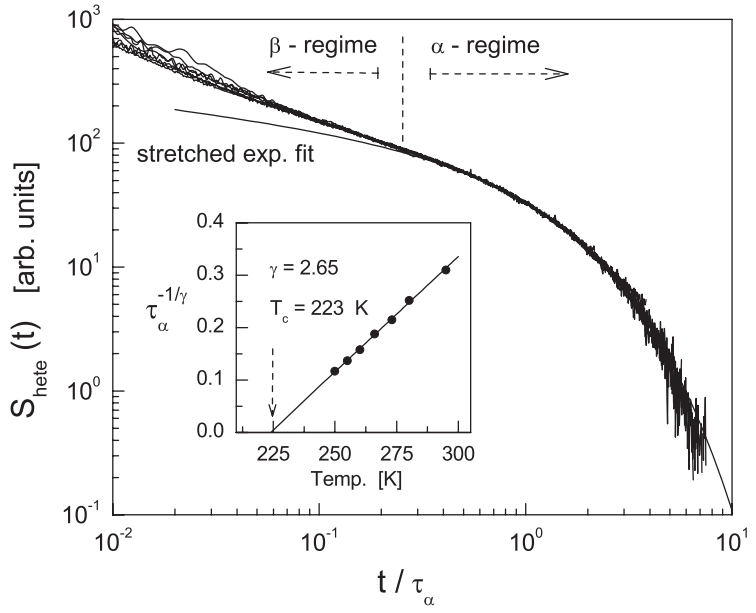

Fig. 2.13 The HD-OKE signals at different temperatures are reported in a master-plot. The time scale of each decay has been divided by a proper τ_α time in order to have the largest overlap possible. A fit according to the derivative of a stretched exponential is shown with $\beta = 0.8$. In the inset, we report the linearized plot of the structural relaxation times vs. temperature

functions should collapse in a single master-function when reported in a rescaled time axis, t/τ_α. In Fig. 2.13, we report the master-plot of m-toluidine data together with temperature dependence of the extracted structural relaxation times. The figure clearly shows that the MCT time–temperature superposition principle holds in the α-regime, enabling a good overlap of OKE data. The linear dependence of structural relaxation times, shown in the inset, proves the validity of the critical law, $\tau_\alpha \propto (T - T_\mathrm{c})^{-\gamma}$, and its fit gives the values of T_c and γ critical parameters.

The intermediate dynamics can be compared with asymptotic MCT predictions of the β-regime. In Fig. 2.14 we report only three OKE plots corresponding to the lower temperatures with the best fit of β-response function, see (2.54). The critical parameters a and b are not temperature dependent and linked by (2.51) to the γ exponent, obtained by the α-regime analysis. The OKE data are well reproduced by the MCT β-correlator for temperature higher than 235 K, corresponding to $T_\mathrm{c} + 10$ K, but for lower temperatures a different relaxation appears in the 2–20 ps time window. This has been addressed, in other glass-formers, as a nearly-logarithmic decay since it would be connected to a logarithmic decay of the correlator [66, 68]. In fact, if $\Phi(t) \approx \log(t)$ we will have $R_\mathrm{oke}(t) \approx t^{-1}$. In our m-toluidine data, we found some evidence of a possible extra power law decay, as shown in Fig. 2.14, with an exponent $c \approx 0.85$.

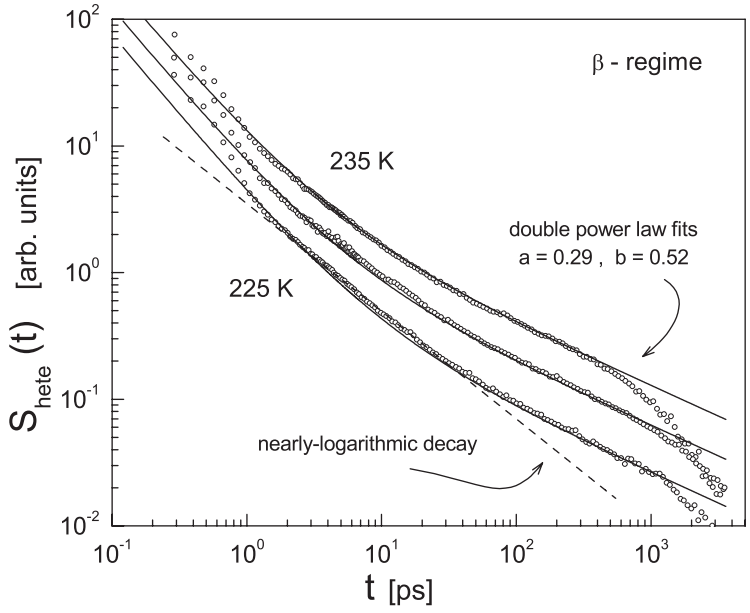

Fig. 2.14 The HD-OKE signals at lower temperatures (225, 229, and 235 K) are reported with a fit according to the derivative of the MCT double power law decay with $b = 0.52$ and $a = 0.29$. An arbitrary vertical shift has been introduced in order to avoid data overlap. In the data decay at 225 K a clear departure from the MCT prediction appears, the presence of a possible nearly-logarithmic decay is evidenced by the dashed line corresponding to a t^{-c} decay with $c \approx 0.85$

In conclusion, we found that the predictions of the schematic MCT model are in very good agreement with the OKE data for weak supercooling but the agreement disappears approaching the critical temperature.

The general experimental scenario of glass-formers for deep supercooling condition is still not clear and there is a live debate on the theoretical models. Concerning the OKE data, this issue has been partially investigated using the schematic two-correlator MCT model [66, 68].

2.5.3 The Water Case

We summarize here our results on supercooled water dynamics by HD-OKE experiments [37]. These results are relevant for two main reasons. First, because they deal with liquid water, one of the most relevant substances in the universe, that presents many anomalous chemical–physical properties. Second, liquid water represents a model system for the investigation of a liquid–liquid phase transition hypothesis.

Many thermodynamic proprieties (such as heat capacity, compressibility, and thermal expansion coefficient) and dynamic properties (such as the shear

viscosity, self-diffusion coefficient, and relaxation times) of water all exhibit an anomalous increase upon cooling [53]. They show a temperature dependence characterized by a diverging power law of the type $(T - T_s)^{-x}$, with $T_s \approx$ 223–228 K. The nature and physical origin of this singularity are still debated, but there are indications of structural modifications occurring around this temperature and the simulation results show that it could be related to the MCT critical temperature.

OKE experiments, as shown in the previous sections, can provide an accurate measure of the relaxation dynamics of molecular liquids, but the intensity of the OKE water signal is very low, making it very difficult to determine its relaxation profile accurately at times longer than a few picoseconds. Here we present the results of an extensive investigation by means of heterodyne detected OKE experiments (HD-OKE) of the relaxation in liquid and supercooled water, using the experimental set-up described in Sect. 2.4. We used optimized laser pulses in order to improve the experimental sensitivity. The entire time decay scan was divided into three sections: short laser pulses (60 fs) were used for the short time scan; for the intermediate time delay intervals the laser pulse duration was stretched up to 120 fs; for the longer time we used stretched laser pulses of 500 fs duration. In this procedure, we increased the pulse energy to keep the peak power roughly constant. The low noise level and the large dynamic range provide data of sufficiently high quality to extend measurements by almost 20° into the supercooled region, up to 254 K. A typical measured signal is shown in Fig. 2.15.

We provided the first unambiguous measurement of the entire correlation function in liquid water as a function of temperature. These data enabled a MCT analysis of the slow dynamic regime. Hence we compared our data with the MCT prediction in the α-regime as already shown for the glass-former liquids.

In Fig. 2.16, we collect all the data measured at different temperatures (314–254 K) in a log–log master-plot. The perfect coincidence of the different curves demonstrates that the slow relaxation of water follows a unique decay law in the entire temperature range considered. We found, for all temperatures, that the time-derivative of the stretched exponential function allows a very satisfactory fitting of the HD-OKE data. The stretching parameter β has a constant value of 0.6 throughout the entire temperature range considered.

As shown in the inset of Fig. 2.16, the temperature dependence of the measured relaxation time τ_α is well reproduced by the MCT power law, $(T - T_c)^{-\gamma}$, with $T_c = 221$ K and $\gamma = 2.2$. So the water singularity temperature $T_s \approx 225$ K, obtained from measurements of other dynamic and transport properties, substantially coincides with the MCT critical temperature.

Two important new results are obtained from our OKE experiment on supercooled water: (1) The stretched exponential nature of the relaxation and the

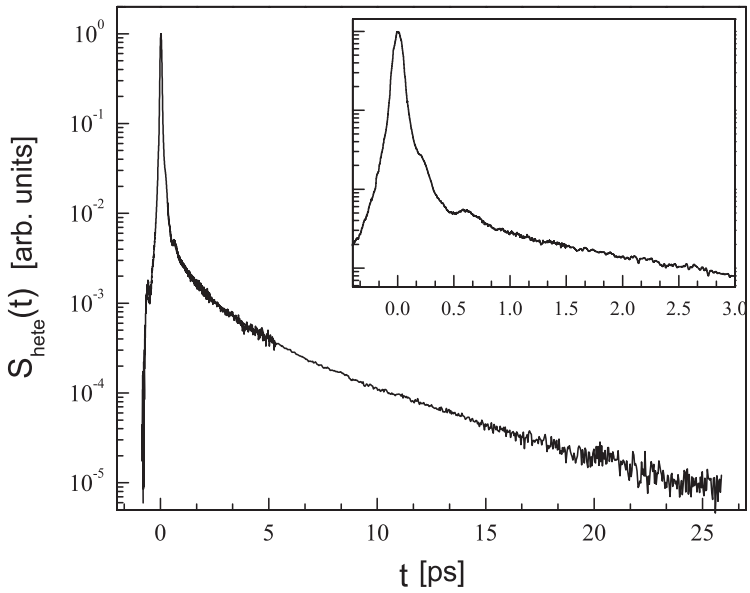

Fig. 2.15 Signal decay measured in the time-resolved HD-OKE experiment on supercooled water at $T = 257$ K. In the inset we reported the signal in the short time region. An oscillatory component occurs in the decay trace for time shorter than 1 ps; for longer times the relaxation shows a monotonic decay

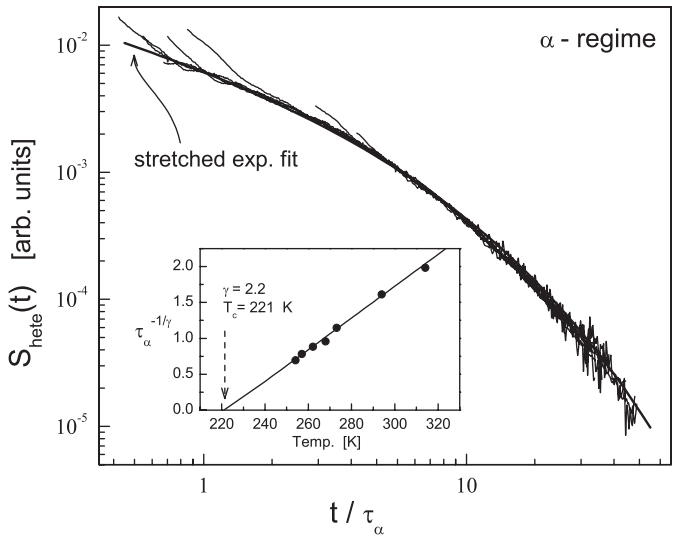

Fig. 2.16 Master plot obtained by rescaling the time and intensity axes of the HD-OKE signals. The inset shows the temperature dependence of the water relaxation times, obtained by the fit of HD-OKE signal decays with the time-derivative of the stretched exponential function

invariance of the stretching parameter with the temperature. The large stretching effect ($\beta = 0.6$) indicates that water dynamics is characterized by a distribution of different timescales, suggesting the presence of a variety of relaxing structures whose distribution does not, according to our results, change notably with temperature. (2) Our data also allow for a comprehensive comparison with the predictions of the MCT model. The MCT predictions agree with our experimental observations, both in terms of the form of the correlation function and in terms of its scaling with temperature.

A purely dynamic water model, as the MCT theory, clearly cannot account for the rich and anomalous thermodynamic behavior of water, which calls for other model types such as the much debated liquid–liquid transition hypothesis [53]. Nevertheless, these OKE results provide with unambiguous evidence that the anomalous behavior of weakly supercooled water at atmospheric pressure can successfully be described by a fully dynamic model, with no need for a thermodynamic origin for the observed anomalous behavior. In this picture the singularity temperature T_{s}, inferred from a range of different dynamic and transport properties of water, is the signature of an avoided dynamical arrest. Despite its strongly hydrogen-bonded nature, weakly supercooled water behaves in this context like a fragile glass-former, similar to many other molecular liquids.

Acknowledgments

The authors wish to thank R. Righini for his fundamental contribution in setting, performing, and understanding of the HD-OKE experiments. We are grateful to R. M. Pick for his continuous support in the glass-former studies. We would like to thank J. Palmer for his critical reading. We acknowledge the scientific encouragement by F. Sciortino and G. Ruocco. Special thanks goes to the technical staff of LENS. The presented research has been performed at LENS and it was also supported by EC grant N.RII3-CT-2003-506350, by CRS-INFM-Soft Matter (CNR), and MIUR-COFIN-2005 grant N. 2005023141-003.

Appendix: Laser Pulses Definition

The laser pulses typically used in an OKE experiment are characterized by an optical frequency (700 nm), a duration longer than 10–20 fs and they are normally transform-limited (i.e., with no time modulation in phase, apart from the optical frequency). The time dependence of the electric field generated by these laser pulses can be safely described as a plane wave in the approximation of the slow parameter variation, see [40]. Hence, using the complex notation we can write the expression of a linearly polarized pulse, as follows

$$\mathbf{E}(\mathbf{r},t) = \hat{\mathrm{e}}_i E_i(\mathbf{r},t) = \hat{\mathrm{e}}_i \mathcal{E}(\mathbf{r},t)\, \mathrm{e}^{\mathrm{i}(\mathbf{k}\cdot\mathbf{r}-\omega t)}, \tag{2.A.1}$$

where $\hat{\mathrm{e}}_i$ is a unit vector indicating the direction of polarization, $\mathbf{k}$ is the wave-vector defining the direction of propagation, ω is the optical frequency, and $\mathcal{E}(\mathbf{r},t)$ defines the pulse envelope. $\mathcal{E}$ is the real, slowly varying time-dependent amplitude defining the pulse time duration, in particular for a continuous laser $\mathcal{E}$ is not time-dependent. Furthermore, it defines the intensity time dependence, since in the complex notation the pulse intensity is given by

$$I(t) \propto |\mathbf{E}(\mathbf{r},t)|^2. \tag{2.A.2}$$

In the experimental configuration defined in Fig. 2.1, the linear polarization of the pump and probe are in the $\hat{x}$ directions and 45° in the $\hat{x}\hat{y}$ plane, respectively. Both the pulses are taken collinear propagating in the $\hat{z}$ direction.

$$\mathbf{E}^{\mathrm{ex}}(z,t) = \hat{\mathrm{e}}_x \mathcal{E}^{\mathrm{ex}}(z,t)\, \mathrm{e}^{\mathrm{i}\omega(\frac{\eta}{c}z-t)}, \tag{2.A.3}$$

$$\mathbf{E}^{\mathrm{pr}}(z,t) = \hat{\mathrm{e}}_x E_x^{\mathrm{pr}}(z,t) + \hat{\mathrm{e}}_y E_y^{\mathrm{pr}}(z,t) = (\hat{\mathrm{e}}_x + \hat{\mathrm{e}}_y)\mathcal{E}^{\mathrm{pr}}(z,t)\, \mathrm{e}^{\mathrm{i}\omega(\frac{\eta}{c}z-t)}. \tag{2.A.4}$$

Here we consider the unique refractive index η, because we are considering two laser beams having the same frequency, ω, and thus propagating with the same phase velocity, $\frac{c}{\eta}$. Furthermore, in these equations we take simply an isotropic index of refraction, considering the beams propagating in the air before the sample, of course the beam polarization does not change during its propagation. For the excitation pulse this applies also during the sample propagation while it does not apply for the probe beam that finds the sample excited, hence an anisotropic index of refraction.

In a typical experiment the probe and excitation pulses are derived from a single laser beam split in two parts of different intensity. Hence the temporal and phase characteristics of the pulses are identical and defined by the main laser beam. Furthermore, in a time-resolved OKE experiment, the probe pulse is delayed by an optical delay that introduces a delay time $\tau = \Delta z \frac{\eta}{c}$, where Δz is the extra length introduced in the probe path. Hence we can write the envelope functions as

$$\mathcal{E}^{\mathrm{ex}}(z,t) = (1-a)\ \mathcal{E}\left(\frac{\eta}{c}z - t\right), \tag{2.A.5}$$

$$\mathcal{E}^{\mathrm{pr}}(z,t) = a\mathcal{E}\left(\frac{\eta}{c}(z+\Delta z) - t\right) = a\mathcal{E}\left(\frac{\eta}{c}z - (t-\tau)\right), \tag{2.A.6}$$

where a is defined by the beam-splitter and the leading envelope function, $\mathcal{E}(t)$, by the main laser and by the group velocity compensation optics. Indeed, the weak anisotropy, induced by the excitation pulse, can be neglected in the envelope propagation (but not in the phase modification). Furthermore this means that the birefringence will be induced and probed with the same time sequence, making the experimental characterization easier [9].

Finally, the laser pulses reaching the sample can be described by the following equations:

$$\mathbf{E}^{\mathrm{ex}}(z,t) \simeq \hat{\mathrm{e}}_x(1-a)\mathcal{E}\left(\frac{\eta}{c}z - t\right)\ \mathrm{e}^{\mathrm{i}\omega\left(\frac{\eta}{c}z-t\right)}, \tag{2.A.7}$$

$$\begin{aligned}\mathbf{E}^{\mathrm{pr}}(z,t) &\simeq (\hat{\mathrm{e}}_x + \hat{\mathrm{e}}_y)\ aE^{\mathrm{pr}}(z,t)\\ &\simeq (\hat{\mathrm{e}}_x + \hat{\mathrm{e}}_y)\ a\mathcal{E}\left(\frac{\eta}{c}z - (t-\tau)\right)\mathrm{e}^{\mathrm{i}\omega\left(\frac{\eta}{c}z-(t-\tau)\right)}.\end{aligned} \tag{2.A.8}$$

Notes

1. The effect of polarizers and other active optical components, on the beam tracking can easily described by the Jones Matrix [73]. According to this picture the two component of the beam, $E_x^{\rm pr}$ and $E_y^{\rm pr}$, are modified by the -45° polarizer matrix, as following:
$\begin{pmatrix} E_x^{\rm sg} & E_y^{\rm sg} \end{pmatrix} = \begin{pmatrix} (E_x^{\rm pr} - E_y^{\rm pr}) & (-E_x^{\rm pr} + E_y^{\rm pr}) \end{pmatrix} = \begin{pmatrix} 1 & -1 \\ -1 & 1 \end{pmatrix} \begin{pmatrix} E_x^{\rm pr} \\ E_y^{\rm pr} \end{pmatrix}$ where the notation $(E_1 E_2) \equiv E_1 \hat{\rm e}_x + E_2 \hat{\rm e}_y$

2. In fact we have $\Delta\eta_{ij}(t) \propto \Delta\chi_{ij}(t) \propto \begin{pmatrix} \int \mathcal{R}_{xxxx} |E^{\rm ex}|^2 & 0 \\ 0 & \int \mathcal{R}_{yyxx} |E^{\rm ex}|^2 \end{pmatrix}$

3. The susceptibility tensor is the proper variable to describe the light-matter interactions, since it links directly the electromagnetic field and the polarization effects. Nevertheless, other variables such as the index of refraction or the dielectric function are very often used in the literature. The Maxwell equations provide the connection between the dielectric tensor, ϵ_{ij}, and the linear susceptibility tensor, χ_{ij} (in literature sometimes called liquid polarizability and reported as Π_{ij}): $\epsilon_{ij} = 1 + 4\pi\chi_{ij}$ in the CGS unit system. It is also straightforward the connection with the index of refraction, since $\eta = \sqrt{\epsilon}$. So when only the fluctuating or time-dependent part is relevant, the three functions are substantially equivalent: $\delta\chi_{ij} \propto \delta\epsilon \propto \delta\eta$

4. This polarizability corresponds to the isolated molecular polarizability normalized over the mean field interaction present in the liquid. It can be substantially different from the molecule polarizability measured in the gas phase.

5. If the pulse is transform limited [40] its spectrum and time profile are directly connected by a Fourier transformation. Hence the spectrum bandwidth is inversely proportional time duration: $\Delta\omega \propto \frac{1}{\Delta\tau}$. For a pulse of 100 fs duration, 100×10^{-15} s, we get a bandwidth of about 30 THz, equivalent to $100\,{\rm cm}^{-1}$. This spectrum width is often large enough to include some intramolecular vibration modes.

6. This expression corresponds to (2.9) at page 172 of the first paper by Pick et al. [49]. Here we neglect the last term of this equation that takes into account the coupling between rotational and slow translational dynamics. This approximation is valid for the limit $q \to 0$, as explicitly shown in Appendix C of that paper.

7. Here we report the simplified version of the MCT asymptotic solutions for the density correlator. They are obtained using the leading-order asymptotic solutions of the MCT. In the α-regime the scaling-law, or *time-temperature superposition principle*, is evident by (2.49). Whereas in the β-regime we do not make explicit the scaling-law that is hidden into (2.50). The rigorous derivation and the full expression of the MCT functions can be found in [60–62]. An experimental comparison between the full β-correlator expression and the next-to-leading order corrections with the OKE signal can be found in [25].

References

[1] Kerr, J. (1875). A new relation between electricity and light: Dielectrified media birefringent. *Philos. Mag.* 50: 336–348, ibidem 446–458. See also Kerr bibliography on (1907) *Nature* 76: 575–576.

[2] Mayer, G. and Gires, R. (1963). The effect of an intense light beam on the index of refraction of liquids. *C.R. Acad. Sci.* 258: 2039.

Marker, P.D., Terhune, R.W. and Savage, C.W. (1964). Intensity-dependent changes in the refractive index of liquids. *Phys. Rev. Lett.* 12: 507–509.

[3] Dugay, M.A. and Hansen, J.W. (1969). An ultrafast light gate. *Appl. Phys. Lett.* 15: 192–194.

Shimuzu, F. and Stoicheff, B.P. (1969). Study of the duration and birefringence of self-trapped filaments in CS_2. *IEEE J. Quantum Electron.* QE-5: 544–546.

[4] Levenson, M.D. and Eesley, G.L. (1979). Polarization selective optical heterodyne detection for dramatically improved sensitivity in laser spectroscopy. *Appl. Phys.* 19: 1–17.

[5] Waldeck, D., Cross, A.J., McDonald, D.B. and Fleming, G.R. (1981). Picosecond pulse induced transient molecular birefringence and dichroism. *J. Chem. Phys.* 74: 3381–3387.

[6] Greene, B.I. and Farrow, R.C. (1983). The subpicosecond Kerr effect in CS_2. *Chem. Phys. Lett.* 98: 273–276.

Greene, B.I., Fleury, P.A., Carter Jr., H.L. and Farrow, R.C. (1984). Microscopic dynamics in simple liquids by sub-picosecond birefringence. *Phys. Rev. A* 29: 271–274.

[7] Kalpouzos, C., Lotshaw, W.T., Mc Morrow, D. and Kenney-Wallace, G.A. (1987). Femtosecond laser-induced Kerr responses in liquid CS_2. *J. Phys. Chem.* 91: 2028–2030.

McMorrow, D., Lotshaw, W.T. and Kenney-Wallace, G.A. (1988). Femtosecond optical Kerr studies on the origin of the nonlinear responses in simple liquids. *IEEE J. Quantum Electron.* QE-24: 443–454.

[8] Lotshaw, W.T., McMorrow, D., Kalpouzos, C. and Kenney-Wallace, G.A. (1987). Femtosecond dynamics of the optical kerr effect in liquid nitrobenzene and chlorobenzene. *Chem. Phys. Lett.* 136: 323–328.

Kalpouzos, C., Lotshaw, W.T., McMorrow, D. and Kenney-Wallace, G.A. (1987). Femtosecond laser-induced Kerr responses in liquid carbon disulfide. *J. Phys. Chem.* 91: 2028–2030.

Kalpouzos, C., McMorrow, D., Lotshaw, W.T. and Kenney-Wallace, G.A. (1989). Femtosecond laser-induced optical Kerr dynamics in CS_2/alkane binary solutions. *Chem. Phys. Lett.* 155: 240–242.

McMorrow, D. and Lotshaw, W.T. (1990). The frequency response of condensed-phase media to femtosecond optical pulses: Spectral-filter effects. *Chem. Phys. Lett.* 174: 85–94.

McMorrow, D. and Lotshaw, W.T. (1991). Dephasing and relaxation in coherently excited ensembles of intermolecular oscillators. *Chem. Phys. Lett.* 178: 69–74.

McMorrow, D. and Lotshaw, W.T. (1993). Evidence for low-frequency ($15\,cm^{-1}$) collective modes in benzene and pyridine liquids. *Chem. Phys. Lett.* 201: 369–376.

McMorrow, D., Thantu, N.J., Melinger, S., Kim, S.K. and Lotshaw, W.T. (1996). Probing the Microscopic Molecular Environment in Liquids: Intermolecular Dynamics of CS_2 in Alkane Solvents. *J. Phys. Chem.* 100: 10389–10399.

[9] Yan, Y. and Nelson, K.A. (1987). Impulsive stimulated light scattering. I. General theory. *J. Chem. Phys.* 87: 6240–6256.

Yan, Y. and Nelson, K.A. (1987). Impulsive stimulated light scattering. II. Comparison to frequency-domain light-scattering spectroscopy. *J. Chem. Phys.* 87: 6257–6265.

[10] Ruhman, S., Williams, L.R., Joly, A.G., Kohler, B. and Nelson, K.A. (1987). Nonrelaxational inertial motion in carbon disulfide liquid observed by femtosecond time-resolved impulsive stimulated scattering. *J. Phys. Chem.* 91: 2237–2240.

Ruhman, S., Joly, A.G. and Nelson, K.A. (1988). Coherent molecular vibrational motion observed in the time-domain through impulsive stimulated Raman scattering. *IEEE J. Quantum Electron.* QE-24: 460–469.

Kohler, B. and Nelson, K.A. (1992). Femtosecond impulsive stimulated light scattering from liquid carbon disulfide at high pressure: Experiment and computer simulation. *J. Phys. Chem.* 96: 6532–6538.

[11] Deeg, F.W., Stankus, J.J., Greenfield, S.R., Newell, V.J. and Fayer, M.D. (1989). Anisotropic reorientational relaxation of biphenyl: Transient grating optical Kerr effect measurements. *J. Chem. Phys.* 90: 6893–6902.

Greenfield, S.R., Sengupta, A., Stankus, J.J., Terazima, M. and Fayer, M.D. (1994). Effects of local liquid structure on orientational relaxation: 2-Ethylnaphthalene, neat and in solution. *J. Phys. Chem.* 98: 313–320.

[12] Palese, S., Schilling, L., Miller, R.J.D., Staver, P.R. and Lotshaw, W.T. (1994). Femtosecond optical Kerr-effect studies of water. *J. Phys. Chem.* 98: 6308–6316.

Palese, S., Mukamel, S., Miller, R.J.D. and Lotshaw, W.T. (1996). Interrogation of vibrational structure and line broadening of liquid water by Raman-induced Kerr-effect measurements within the multimode Brownian oscillator model. *J. Phys. Chem.* 100: 10380–10388.

[13] Waldman, A., Banin, U., Rabani, E. and Ruhman, S. (1992). Temperature dependence of light scattering from neat benzene with femtosecond pulses: Are we seeing molecules librate? *J. Phys. Chem.* 96: 10842–10848.

[14] Cho, M., Du, M., Scherer, N.F., Fleming, G.R. and Mukamel, S. (1993). Off-resonance birefringence in liquids. *J. Chem. Phys.* 99: 2410–2428.

[15] Righini, R. (1993). Ultrafast optical Kerr effects in liquids and solids. *Science* 262: 1386–1390.

Foggi, P., Bellini, M., Kien, D.P., Vercuque, I. and Righini, R. (1997). Relaxation dynamics of water and HCl aqueous solutions measured by time-resolved optical Kerr effect. *J. Phys. Chem.* 101: 7029–7035.

Ricci, M., Bartolini, P., Chelli, R., Cardini, G., Califano, S. and Righini, R. (2001). The fast dynamics of benzene in the liquid phase, Part I: Optical Kerr effect experimental investigation. *Phys. Chem. Chem. Phys.* 3: 2795–2802.

[16] Chang, Y.J. and Castner Jr., E.W. (1993). Femtosecond dynamics of hydrogen-bonding solvents. Formamide and N-methylformamide in acetonitrile, DMF, and water. *J. Chem. Phys.* 99: 113–125.

Chang, Y.J. and Castner Jr., E.W. (1993). Fast responses from "slowly relaxing" liquids: A comparative study of the femtosecond dynamics of triacetin, ethylene glycol, and water. *J. Chem. Phys.* 99: 7289–7299.

Castner Jr., E.W., Chang, Y.J., Chu, Y.C. and Walrafen, G.E. (1995). The intermolecular dynamics of liquid water. *J. Chem. Phys.* 102: 653–659.

Chang, Y.J. and Castner Jr., E.W. (1996). Intermolecular dynamics of substituted benzene and cyclohexane liquids, studied by femtosecond nonlinear-optical polarization spectroscopy. *J. Phys. Chem.* 100: 3330–3343.

[17] Deuel, H.P., Cong, P. and Simon, J.D. (1994). Probing intermolecular dynamics in liquids by femtosecond optical Kerr effect Spectroscopy: Effects of molecular symmetry. *J. Phys. Chem.* 98: 12600–12608.

Cong, P., Deuel, H.P. and Simon, J.D. (1995). Structure and dynamics of molecular liquids investigated by optical-heterodyne detected Raman-induced Kerr effect spectroscopy (OHD-RIKES). *Chem. Phys. Lett.* 240: 72–78.

Chang, Y.J., Cong, P. and Simon, J.D. (1995). Optical heterodyne detection of impulsive stimulated Raman scattering in liquids. *J. Phys. Chem.* 99: 7857–7859.

Cong, P., Chang, Y.J. and Simon, J.D. (1996). Complete determination of intermolecular spectral densities of liquids using position-sensitive Kerr lens spectroscopy. *J. Phys. Chem.* 100: 8613–8616.

[18] Quivetis, E.L. and Neelakandam, M. (1996). Femtosecond optical Kerr effect studies of liquid methyl iodide. *J. Phys. Chem.* 100: 10005–10014.

[19] Bartolini, P., Ricci, M., Torre, R. and Righini, R. (1999). Diffusive and oscillatory dynamics of liquid iodobenzene measured by femtosecond optical Kerr effect. *J. Chem. Phys.* 110: 8653–8659.

[20] Loughnane, B., Scodinu, A., Farrer, R.A. Fourkas, J.T. and Mohanty, U. (1999). Exponential intermolecular dynamics in optical Kerr effect spectroscopy of small-molecule liquids. *J. Chem. Phys.* 111: 2686–2694.

Loughnane, B., Scodinu, A. and Fourkas, J.T. (2006). Temperature-dependent optical Kerr effect spectroscopy of aromatic liquids. *J. Phys. Chem. B* 110: 5708–5720.

[21] Voehringer, P. and Scherer, N.F. (1995). Transient grating optical heterodyne detected impulsive stimulated Raman scattering in simple liquids. *J. Phys. Chem.* 99: 2684–2695.

Winkler, K., Lindner, J., Buoersing, H. and Voehringer, P. (2000). Ultrafast Raman-induced Kerr-effect of water: Single molecule versus collective motions. *J. Chem. Phys.* 113:4674–4682.

Winkler, K., Lindner, J. and Voehringer, P. (2002). Low frequency depolarized Raman-spectral density of liquid water from femtosecond optical Kerr-effect measurements: Lineshape analysis of restricted translational modes. *Phys. Chem. Chem. Phys.* 4: 2144–2155.

[22] Torre, R., Santa, I. and Righini, R. (1993). Pre-transitional effects in the liquid-plastic transition of p-terphenyl. *Chem. Phys. Lett.* 212:90–95.

Torre, R. and Califano, S.(1996). Local order effect on molecular orientational dynamics: Time resolved non-linear spectroscopy. *J. Chim. Phys.* 93:1843–1857.

[23] Stankus, J.J., Torre, R. and Fayer, M.D. (1993). Influence of local liquid structure on orientational dynamics: Isotropic phase of liquid crystals. *J. Chem. Phys.* 97: 9480–9487.

Torre, R., Ricci, M., Saielli, G., Bartolini, P. and Righini, R. (1995). Orientational Dynamics in the isotropic phase of a nematic mixture: Subpicosecond time resolved optical Kerr effect experiments on ZLI-1167 liquid crystal. *Mol. Cryst. Liq. Cryst.* 262: 391–402.

Torre, R., Tempestini, F., Bartolini, P. and Righini, R. (1995). Collective and single particle dynamics near the isotropic-nematic phase transition. *Philos. Mag. B* 77: 645–653.

[24] Torre, R., Bartolini, P. and Pick, R.M. (1998). Time-resolved optical Kerr effect in a fragile glass-forming liquids, salol. *Phys. Rev. E* 57: 1912–1920.

[25] Torre, R., Bartolini, P., Ricci, M. and Pick, R.M. (2000). Time-resolved optical Kerr effect on a fragile glass-forming liquid: Test of different mode-coupling theory aspects. *EuroPhys. Lett.* 52: 324–329.

[26] Hinze, G., Brace, D.D., Gottke, S.D. and Fayer, M.D. (2000). A detailed test of mode-coupling theory on all time scales: Time domain studies of structural relaxation in a supercooled liquid. *J. Chem. Phys.* 113: 3723–3733.

[27] Ricci, M., Bartolini, P. and Torre, R. (2002). Fast dynamics of a fragile glass-former by time resolved spectroscopy. *Philos. Mag. B* 82: 541–551.

[28] Prevosto, D., Bartolini, P., Torre, R., Ricci, M., Taschin, A., Capaccioli, S., Lucchesi, M. and Rolla, P. (2002). Relaxation processes in a epoxy resin studied by time resolved optical Kerr effect. *Phys. Rev. E* 66: 011502 (1–12).

[29] Pratesi, G., Bartolini, P., Senatra, D., Ricci, M., Righini, R., Barocchi, F. and Torre, R. (2003). Experimental studies of the ortho-toluidine glass transition. *Phys. Rev. E* 67: 021505(1–8).

[30] Cang, H., Novikov, V.N. and Fayer, M.D. (2003). Experimental observation of a nearly logarithmic decay of the orientational correlation function in supercooled liquids on the picosecond-to-nanosecond time scales. *Phys. Rev. Lett.* 90: 197401(1–4).

[31] Hinze, G., Francis, R. and Fayer, M.D. (1999). Translational–rotational coupling in supercooled liquids: Heterodyne detected density induced molecular alignment. *J. Chem. Phys.* 111:2710–2719.

[32] Elschner, R., Macdonald, R., Eichler, H.J., Hess, S. and Sonnet, A.M. (1999). Molecular reorientation of a nematic glass by laser-induced heat flow. *Phys. Rev. E* 60: 1792–1797.

[33] Torre, R., Taschin, A. and Sampoli, M. (2001). Acoustic and relaxation processes in supercooled o-ter-phenyl by optical-heterodyne transient grating experiment. *Phys. Rev. E* 64: 61504(1-10).

[34] Taschin, A., Torre, R., Ricci, M., Sampoli, M., Dreyfus, C., Pick. and R.M. (2001). Translational-rotation coupling in transient grating experiments: Theoretical and experimental evidences. *EuroPhys. Lett* 53: 407–413.

[35] Glourieux, C., Hinze, G., Nelson, K.A. and Fayer, M.D. (2002). Thermal, structural, and orientational relaxation of supercooled salol studied by polarization-dependent impulsive stimulated scattering. *J. Chem. Phys.* 116: 3384–3395.

[36] Ricci, M., Wiebel, S., Bartolini, P., Taschin, A. and Torre, R. (2004). Time-resolved optical Kerr effect experiments on supercooled benzene and test of mode-coupling theory. *Philos. Mag.* 84: 1491–1498.

[37] Torre, R., Bartolini, P. and Righini, R. (2004). Structural relaxation in supercooled water by time-resolved spectroscopy. *Nature* 428: 296–299.

[38] Constantine, S., Zhou, Y., Morais, J. and Zigler, L.D. (1997). Dispersed optical heterodyne detected birefringence and dichroism of transparent liquids. *J. Phys. Chem. A* 101: 5456–5462.

[39] Bloembergen, N. (1965). *Nonlinear optics*. W.A. Benjamin, New York.

[40] Shen, Y.R. (1984). *The principles of nonlinear optics*. Wiley, New York.

[41] Hellwarth, R.W. (1977). Third-order optical susceptibilities of liquids and solids. *Prog. Quantum Electron.* 5:1–68.

[42] Berne, B.B. and Pecora, R. (1976). *Dynamic light scattering*. Wiley, New York.

[43] Kubo, R., Toda, M. and Hashitsume, N. (1992). *Statistical Physics I and II*. Series on Solid-State Science, vol.31, Springer-Verlag, Berlin.

[44] Madden, P.A. (1991). Molecular motion in liquids. In Hansen, J.P., Levesque, D., and Zinn-Justin, J., editors, *Liquids, freezing and glass transition*, Les Houches 1989, Session LI, pages 551–624, North-Holland, Amsterdam.

[45] Latz, A. and Letz, M. (2001). On the theory of light scattering in molecular liquids. *Eur. Phys. J. B* 19: 323–343.

[46] Ladanyi, B.M. and Klein, S. (1996). Contributions of rotation and translation to polarizability anisotropy and solvation dynamics in acetonitrile. *J. Chem. Phys.* 105: 1552–1561.

[47] Murry, R.L., Fourkas, J.T. and Keyes, T. (1998). Nonresonant intermolecular spectroscopy beyond the Placzek approximation. I. Third-order spectroscopy. *J. Chem. Phys.* 109: 2814–2825.

[48] Pick, R.M., Franosch, T., Latz, A. and Dreyfus, C. (2003). Light-scattering by longitudinal phonons in molecular supercooled liquids. I. Phenomenological approach. *Eur. Phys. J. B* 31:217–229.

Franosch, T., Latz, A. and Pick, R.M. (2003). Light-scattering by longitudinal phonons in molecular supercooled liquids. II. The Microscopic Derivation of the phenomenological equations. *Eur. Phys. J. B* 31:229–246.

[49] Pick, R.M., Dreyfus, C., Azzimani, A., Gupta, R., Torre, R., Taschin, A. and Franosch, T. (2004). Heterodyne detected transient gratings in supercooled molecular liquids. A phenomenological theory. *Eur. Phys. J. B* 39:169–197.

Franosch, T. and Pick, R.M. (2005). Transient grating experiments on supercooled molecular liquids. II. Microscopic derivation of the phenomenological equations. *Eur. Phys. J. B* 47: 341–361.

[50] Gray, C.G. and Gubbins, K.E. (1984). *Theory of molecular fluids*. Clarendon Press, Oxford.

[51] Hansen, J.P. and McDonald, I.R. (1986). *Theory of simple liquids*. Academic Press, London.

[52] Balucani, U. and Zoppi, M. (1994). *Dynamics of the liquid state*. Clarendon Press, Oxford.

[53] DeBenedetti, P.G. (1996). *Metastable liquids*. Princeton University Press, New Jersey.

[54] Landau, L.D. and Lifhsitz, E.M. (1959). *Fluids mechanics*. Pergamon Press, London.

[55] Boon, J.P. and Yip, S. (1980). *Molecular hydrodynamics*. McGraw-Hill, New York.

[56] Wang, C.H. (1985). *Spectroscopy of condensed media*. Academic Press, New York.

[57] Mukamel, S. (1995). *Principles of non linear optical spectroscopy*. Oxford University Press, New York.

[58] Chelli, R., Cardini, G., Ricci, M., Bartolini, P., Righini, R. and Califano, S. (2001). The fast dynamics of benzene in the liquid phase, Part II: A molecular dynamics simulation. *Phys. Chem. Chem. Phys.* 3: 2803–2810.

[59] Ryu, S. and Stratt, R.M. (2004). A case study in the molecular interpretation of optical Kerr effect spectra: Instantaneous-normal-mode analysis of the OKE spectrum of liquid benzene. *J. Phys. Chem. B* 108: 6782–6795.

[60] Götze, W. (1991). Aspects of structural glass relaxations. In Hansen, J.P., Levesque, D., and Zinn-Justin, J., editors, *Liquids, freezing and glass transition*, Les Houches 1989, Session LI, pages 287–499, North-Holland, Amsterdam.

Götze, W. and Sjögren, L. (1992). Relaxation processes in supercooled liquids. *Rep. Prog. Phys.* 55: 241–376.

[61] Kob, W. (1996). Theoretical perspectives on supercooled liquids. In Fourkas, J.T., Kivelson, D., Mohanty, U. and Nelson, K.A., editors, *Supercooled Liquids*, ACS Symposium Series, p. 28–44. Princeton University Press, New Jersey.

[62] Cummins, H.Z. (1999). The liquid–glass transition: A mode-coupling perspective. *J. Phys. Condens. Matter* 11: A95–A117.

[63] Keyes, T. and Kivelson, D. (1972). Depolarized light scattering: Theory of the sharp and broad Rayleigh lines. *J. Chem. Phys.* 56: 1057–1065.

[64] Moro, G.J., Nordio, P.L., Noro, M. and Polimeno, A. (1994). A cage model of liquids supported by molecular dynamics simulations. I. The cage variables. *J. Chem. Phys.* 101: 693–702.

Polimeno A. and Moro, G.J. (1994). A cage model of liquids supported by molecular dynamics simulations. II. The stochastic model. *J. Chem. Phys.* 101: 703–712.

[65] Götze, W. (1999). Recent tests of the mode-coupling theory for glassy dynamics. *J. Phys. Condens. Matter* 11: A1–A45.

[66] Götze, W. and Sperl, M. (2004). Nearly-logarithmic decay of correlations in glass-forming liquids. *Phys. Rev. Lett.* 92: 105701.

[67] L. Sjögren (1986). Diffusion of impurities in a dense fluid near the glass transition. *Phys. Rev. A* 33:1254–1260.

Götze, W. and Voigtmann, Th. (2000). Universal and non-universal features of glassy relaxation in propylene carbonate. *Phys. Rev. E* 61: 4133–4145.

Chong, S.-H. and Götze, W. (2002). Structural relaxation in a system of dumbbell molecules. *Phys. Rev. E* 65: 051201.

[68] Sperl, M. (2006). Cole-Cole law for critical dynamics in glass-forming liquids. *Phys. Rev. E* 74: 011503(1–15).

[69] Dies, J.C. and Rudolph, W. (1996). *Ultrashort laser pulse phenomena*. Academic Press, San Diego.

[70] Bartolini, P., Eramo, R., Taschin, A., De Pas, M. and Torre, R. (2007). A real-time acquisition system for pump-probe spectroscopy. *Philos. Mag.* 87:731–740.

[71] Giraud, G., Gordon, C.M., Dunkin, I.R. and Wynne, K. (2003). The effects of anion and cation substitution on the ultrafast solvent dynamics of ionic liquids: A time-resolved optical Kerr-effect spectroscopic study. *J. Chem. Phys.* 119: 464–477.

[72] Bartolini, P., Eramo, R., Taschin, A. and Torre, R. (2007). A super-heterodyne-detected optical-Kerr-effect study of supercooled water dynamics. In preparation.

[73] Lotshaw, W.T., Mc Morrow, D., Thantu, N., Melonger, J.S. and Kitchenham, R. (1995). Intermolecular vibrational coherence in molecular liquids. *J. Raman Spectrosc.* 26: 571–583.

[74] Kinoshita, S., Kai, Y., Yamaguchi, M. and Yagi, T. (1995). Direct comparison between ultra-fast optical Kerr effect and high-resolution light scattering spectroscopy. *Phys. Rev. Lett.* 75: 148–151.

[75] Brodin, A. and Rössler, A.E. (2006). Depolarized light scattering versus optical Kerr effect spectroscopy of supercooled liquids: Comparative analysis. *J. Chem. Phys.* 125: 114502(1-9).

http://www.springer.com/978-0-387-25557-6

Time-Resolved Spectroscopy in Complex Liquids
An Experimental Perspective
Torre, R. (Ed.)
2008, XII, 252 p. 97 illus., Hardcover
ISBN: 978-0-387-25557-6